Meteoritics & Planetary Science 42, Nr 6, 913–933 (2007)
Abstract available online at http://meteoritics.org

Microstructure and thermal history of metal particles in CH chondrites

J. I. GOLDSTEIN[1*], R. H. JONES[2], P. G. KOTULA[3], and J. R. MICHAEL[3]

[1]Department of Mechanical and Industrial Engineering, 313 Engineering Laboratory,
University of Massachusetts, 160 Governors Drive, Amherst, Massachusetts 01003, USA
[2]Department of Earth and Planetary Sciences, University of New Mexico, Albuquerque, New Mexico 87131, USA
[3]Materials Characterization Department, Sandia National Laboratories,
P.O. Box 5800, M.S. 0886, Albuquerque, New Mexico 87185, USA
[*]Corresponding author. E-mail: jig0@ecs.umass.edu

(Received 30 August 2006; revision accepted 27 January 2007)

Abstract–We have studied metal microstructures in four CH chondrites, Patuxent Range (PAT) 91546, Allan Hills (ALH) 85085, Acfer 214, and Northwest Africa (NWA) 739, to examine details of the thermal histories of individual particles. Four types of metal particles are common in all of these chondrites. Zoned and unzoned particles probably formed as condensates from a gas of chondritic composition in a monotonic cooling regime, as has been shown previously. We have demonstrated that these particles were cooled rapidly to temperatures below 500 K after they formed, and that condensation effectively closed around 700 K. Zoned and unzoned particles with exsolution precipitates, predominantly high-Ni taenite, have considerably more complex thermal histories. Precipitates grew in reheating episodes, but the details of the heating events vary among individual grains. Reheating temperatures are typically in the range 800–1000 K. Reheating could have been the result of impact events on the CH parent body. Some particles with precipitates may have been incorporated into chondrules, with further brief heating episodes taking place during chondrule formation. In addition to the four dominant types of metal particles, rare Ni-rich metal particles and Si-rich metal particles indicate that the metal assemblage in CH chondrites was a mixture of material that formed at different redox conditions. Metal in CH chondrites consists of a mechanical mixture of particles that underwent a variety of thermal histories prior to being assembled into the existing brecciated meteorites.

INTRODUCTION

The CH chondrites are a group of metal-rich carbonaceous chondrites. Their chondrules are small, and they have a high abundance of cryptocrystalline chondrules, a high abundance of metal (up to 20 vol%), a low abundance of sulfide (<1 vol%), and a unique suite of calcium-aluminum-rich inclusions (CAIs). CH chondrites are related to other metal-rich chondrites (CR and CB meteorites) that are collectively known as the "CR clan" (Weisberg et al. 1995; Krot et al. 2002). There are two types of CH chondrites. The Allan Hills (ALH) 85085–like chondrites have mean chondrule diameters of 20 μm (Grossman et al. 1988; Scott 1988; Weisberg et al. 1988; Wasson and Kallemeyn 1990). Two chondrites, Acfer 182 (Bischoff et al. 1993) and Northwest Africa (NWA) 739 (Jones et al. 2005), are similar to each other and are characterized by larger chondrules (mean diameter 90 μm) and significantly different oxygen isotopic compositions from the ALH 85085–like group. Currently these two chondrites are included in the CH group, although Weisberg et al. (1995) argued that Acfer 182 was sufficiently different from the other CH chondrites that it should be considered a unique chondrite.

The origin of CH chondrites is the subject of some debate: characteristics of CAIs, chondrules, and metal grains indicate condensation from the nebula gas (Grossman et al. 1988; Scott 1988; Weisberg et al. 1988; Meibom et al. 1999a, 2000; Krot et al. 2001; Petaev et al. 2003; Hezel et al. 2003; Campbell and Humayun 2004) whereas other characteristics, such as high metal abundances, have been argued to support an origin in an impact plume in the nebula (Wasson and Kallemeyn 1990). Understanding whether metal in CH chondrites formed, for example, in a solar nebular gas or within an impact plume is critical to interpreting the formation of the entire CH chondrite (e.g., Campbell et al. 2005a).

Fe-Ni metal particles with smooth Ni, Co, and Cr zoning patterns, 8–13 wt% Ni in the center of the particle to

3–5 wt% Ni at the rim, have been identified in several CR-clan chondrites (Meibom et al. 1999a; Campbell and Humayun 2004; Campbell et al. 2005a). These zoning patterns are broadly consistent with an origin by gas-solid condensation in the solar nebula. Initial estimates yield gas-solid condensation at pressures of 10^{-4} bars, temperatures between ~1500 to 1300 K, and cooling rates from 2 to 25 K/day (Meibom et al. 2000; Petaev et al. 2003). Minor- and trace-element compositions in zoned metal grains in CH chondrites also correlate with Ni in a manner that strongly indicates that the elemental distributions are controlled by the volatility of each element (Campbell et al. 2005a). Apparently, zoned condensate metal was not melted during chondrule formation or affected significantly in the solid state by alteration during parent body processing. Consideration of diffusional redistribution of Ni, Co, Cr, and siderophile elements have further constrained the calculated condensation temperatures (1360 to ~1250 K) and cooling rates of the zoned condensates (Petaev et al. 2003; Campbell and Humayun 2004). These condensate metals have irregular shapes and vary in size from 50 to 350 μm as revealed in some detail by optical and scanning electron microscopy (SEM) techniques (Reisener et al. 2000; Leroux and Perron 2001). In addition to zoned condensate particles, other types of metal particles have been observed. These include zoned condensates with exsolution-precipitates (Meibom et al. 1999a; Campbell and Humayun 2004), unzoned homogeneous metal with no exsolution-precipitates (Campbell and Humayun 2004; Meibom et al. 1999b), unzoned metal exhibiting exsolution-precipitates (Meibom et al. 1999b; Campbell and Humayun 2004) and high-Ni metal grains (Meibom et al. 1999b). The unzoned metal grains were most likely formed by later stage condensation from a solar gas after removal of zoned metal (Campbell and Humayun 2004).

The purpose of this study is to obtain detailed microstructural and microchemical information at the nanometer-to-micrometer scale for a select suite of metal particles in CH chondrites. Using information such as the degree of exsolution and textural observations, we are able to determine temperature-time relationships for formation of individual particles, and the effect of shock-mechanical deformation. We also examine the relationship between various types of metal particles and the variation of particle type within and among the different CH chondrites.

PROCEDURE

Twenty-four metal particles from four CH chondrites, Patuxent Range (PAT) 91546, Allan Hills (ALH) 85085, Acfer 214, and Northwest Africa (NWA) 739, were selected for detailed microstructural analysis. Demountable thin sections of PAT 91546 and ALH 85085 were obtained from the Meteorite Working Group. A demountable thin section of Acfer 214 (paired with Acfer 182) and a polished mount of NWA 739 (UNM 1128) were obtained from the University of New Mexico (UNM) meteorite collection.

Sections of the four chondrites were prepared for metallographic analysis. The samples were polished with diamond paste (6, 3, 1, and 0.25 μm) and etched in 2% nital. Optical and scanning electron microscopy were employed to determine the microstructure of the metal particles, for example, the presence or absence of precipitates, recrystallized grains, mechanical deformation, etc. A JEOL 8200 electron probe microanalyzer (EPMA) with 5 wavelength dispersive spectrometers at the University of New Mexico was employed for X-ray scanning and for quantitative analysis of Fe, Ni, Co, P, Cr, Si, and S in metal particles, using an accelerating voltage of 15kV and beam currents of 20–40 nA (for quantitative analysis) and 100nA (for X-ray mapping). Quantitative analysis used a ZAF correction procedure and included background subtraction corrections for peak overlaps, including the interference of Fe Kβ with Co Kα peaks. Quantitative chemical analyses of micron-size regions of the metal particles were obtained point by point along a line across the metal particles. A dual-beam FEI DB-235 focused ion beam (FIB)/SEM instrument at Sandia National Laboratories (SNL) was used to obtain TEM thin samples (50–100 nm thick) approximately 10 μm long and 5 μm deep from 10 CH metal particles. These TEM samples were taken along selected portions of the quantitative line scans obtained using the EPMA. Selected regions of the 10 metal particles were analyzed using a FEI Tecnai F30ST field emission transmission–analytical electron microscope (TEM-AEM), also at SNL, operated at 300keV. X-ray spectral images (complete spectra from each point of a 2-D array of points) were taken in micron-size regions of the thin foil. Quantitative X-ray analyses were obtained from the X-ray spectral image data using multivariate curve resolution methods (Keenan et al. 2003; Keenan et al. 2004; Kotula et al. 2003; Kotula et al. 2006) on the spectral images, over the range of energies from 6 kV to 9 kV, to extract the Fe and Ni, Kα and Kβ intensities, followed by the Cliff Lorimer method (Cliff and Lorimer 1975) with X-ray spatial resolution, in some cases, better than 2 nm. A $k_{Fe\text{-}Ni}$ factor in the Cliff Lorimer method of 1.10 was measured at 300 keV using a 25 wt% Ni-Fe standard. Electron backscatter diffraction (EBSD) using a field emission ZEISS Supra 55VP SEM, outfitted with an EBSD unit from HKL and Channel 6 software, was employed to determine orientation relationships in recrystallized metal grains.

We used the calculation procedures developed by Smith and Goldstein (1977) to estimate the temperature-time relationships for the formation of the microstructure of individual particles. Heating temperatures were obtained by measuring the composition of the exsolved or reheated taenite phase. Cooling rates and final equilibration temperatures were estimated after measurement of the compositions of kamacite and taenite at two phase interfaces. The time at the

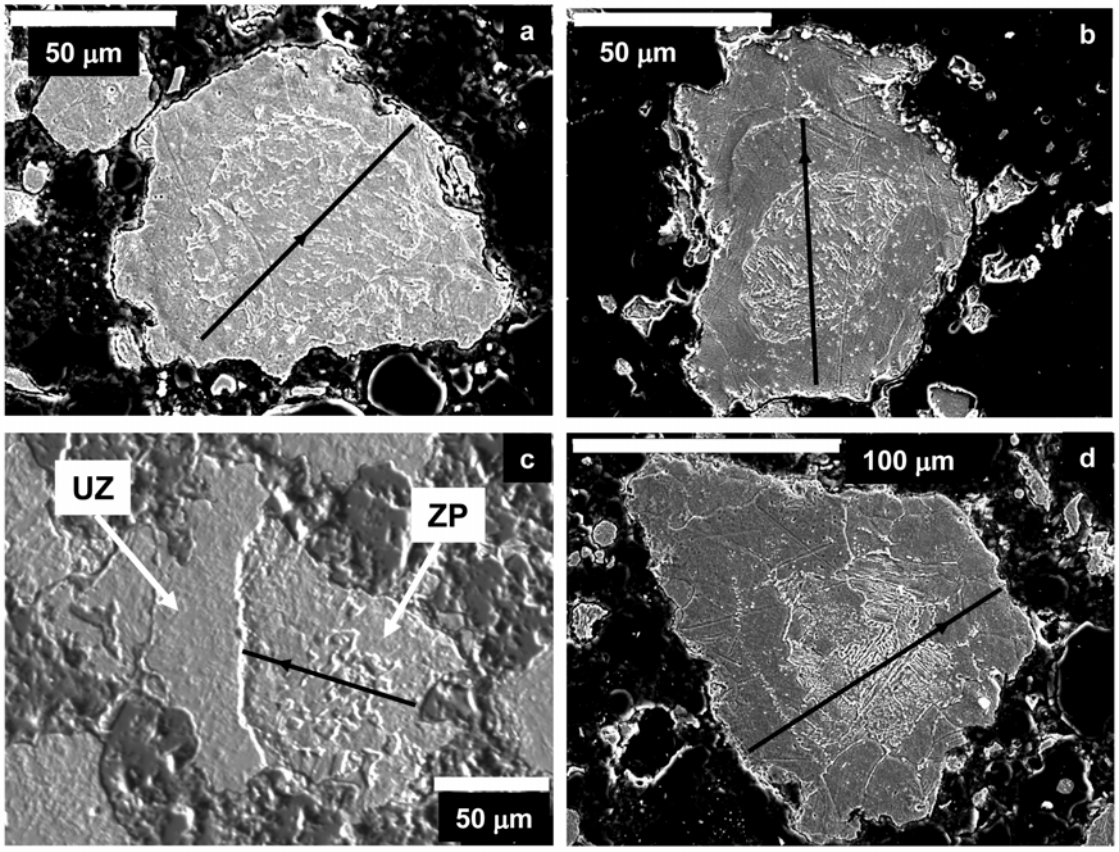

Fig. 1. a) and b) Microstructures of two zoned metal particles (Z) as observed in the SEM with secondary electrons. a) Metal grain A2 in PAT 91546. b) Metal grain C1 in ALH 85085. The microstructure in the center of particles PAT A2 and ALH C1 is martensite, α_2, surrounded by a featureless region of kamacite. c) and d) Microstructures of two zoned metal particles with precipitates (ZP). c) Metal grain A2 in NWA 739. d) Metal grain B2 in PAT 91546. (c) also shows unzoned (UZ) particle A2H, which is attached to metal grain A2. The microstructure in the center of particles NWA 739 A2 and PAT 91546 B2 is martensite, α_2, with precipitates of taenite, γ. The microstructure in the center of the particles is surrounded by a featureless region of kamacite. The line across each particle indicates the position where EPMA data were collected.

reheating or decomposition temperature was obtained by measuring the size of the exsolved or reheated taenite. The size of the phase X is related to the time t of reheating or decomposition at a specific temperature through the relation:

$$X \sim (Dt)^{1/2} \quad (1)$$

where D is the diffusion coefficient of Ni in the matrix kamacite phase. The most current values of D are given by Yang and Goldstein (2006).

RESULTS

Five types of metal particles (zoned, zoned with exsolution-precipitates, unzoned metal, unzoned metal exhibiting exsolution-precipitates, and high-Ni metal grains) 20 to 200 μm in size were analyzed in PAT 91546, NWA 739, ALH 85085, and Acfer 214. The following sections present the metallography of these particles as well as X-ray area maps and quantitative microchemistry obtained from the EPMA, SEM-EBSD, and TEM-AEM.

Zoned Metal (Z)

The central regions of the zoned condensate particles are enriched in Ni and Co and depleted in Cr and Fe, as described in previous studies (Meibom et al. 1999a; Campbell and Humayun 2004). Figure 1a shows the microstructure of a 100 × 100 μm metal grain A2 in PAT 91546, and Fig. 1b shows the microstructure of a 90 × 60 μm metal grain C1 in ALH 85085. The microstructure in the center of particles PAT A2 and ALH C1 is martensite, α_2, which is surrounded by a featureless region of kamacite with a Ni content less than ~7 wt%. Figures 2a–d display the variation of Fe, Ni, Co, Cr, and P across four zoned condensate metal particles measured with the EPMA. Ni zoning is observed in all four particles. The extent of the Ni zoning varies from a factor of >2 in ALH C2 to a factor of 1.3 in ALH C1. The extent of the Ni zoning and the maximum Ni content may be a function of how the metal particle was sectioned for analysis (close to or far away from the center of the particle). Figures 3a–d display X-ray scanning maps which show the variation of Ni, Cr, S, and P

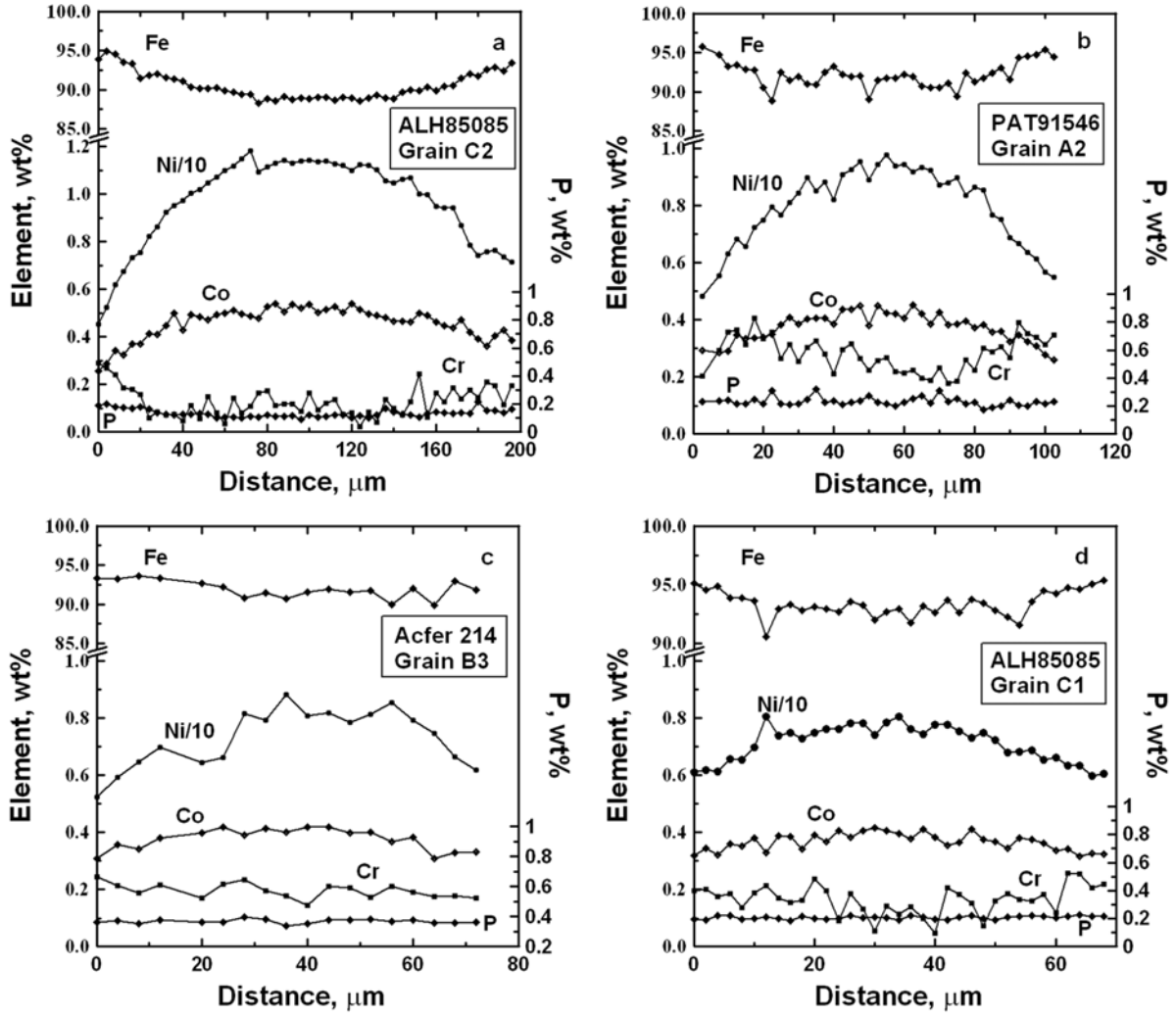

Fig. 2. a–d) Variation of Fe, Ni, Co, Cr, and P across four zoned metal particles (Z) measured with the EPMA. Ni zoning is observed in all four particles.

across particle ALH C1. The data are consistent with the EPMA data of Fig. 2, where the Ni varies from 6 wt% at the outside of the particle increasing to ~8 wt% in the center of the particle, Co follows the Ni from 0.30 to 0.42 wt%, Cr decreases with increasing Ni from 0.26 to 0.05 wt%, and P is ~0.2 wt% across the particle. No sulfides were observed in the microstructure (Fig. 3b) and the S content, as measured with the EPMA, is less than 0.01 wt%. Figures 4a–c illustrate the strong correlation between Co and Ni along the C1 solar line in the four zoned condensate particles. In addition, Cr and P vary inversely with Ni content in ALH C2 and Acfer B3 and P is independent of Ni content in PAT A2 and ALH C1.

Quantitative X-ray analysis obtained from the EPMA shows that the metal particles have continuous composition gradients at the micron level. Presumably no precipitates have formed and no plastic deformation has taken place at the micron level due to shock or heat treatment during formation of the metal particles. To determine if more subtle phase transformations or shock structures have formed at the submicron level, we made electron transparent thin sections for observation in the transmission electron microscope (TEM). Figure 5 shows the microstructure obtained using the TEM (annular dark-field STEM image) from a 4 × 4 μm region at the center of particle ALH C1 along the direction of the EPMA trace where the average Ni content is ~8 wt%. The microstructure is lath martensite and the boundaries observed in the photomicrograph delineate the various laths or regions of martensite. No precipitates are observed in the TEM section (Fig. 5), or in a 500 × 500 nm X-ray scan at a pixel size of 4 nm. In addition, a TEM sample taken from the center of particle PAT A2 also had a lath martensite structure and there was no evidence of precipitates at a pixel size of 16 nm. Using the methodology of Smith and Goldstein (1977), we estimate that these particles could not have been reheated to 1000 K for more than 1 s, 900 K for more than 1 min, or

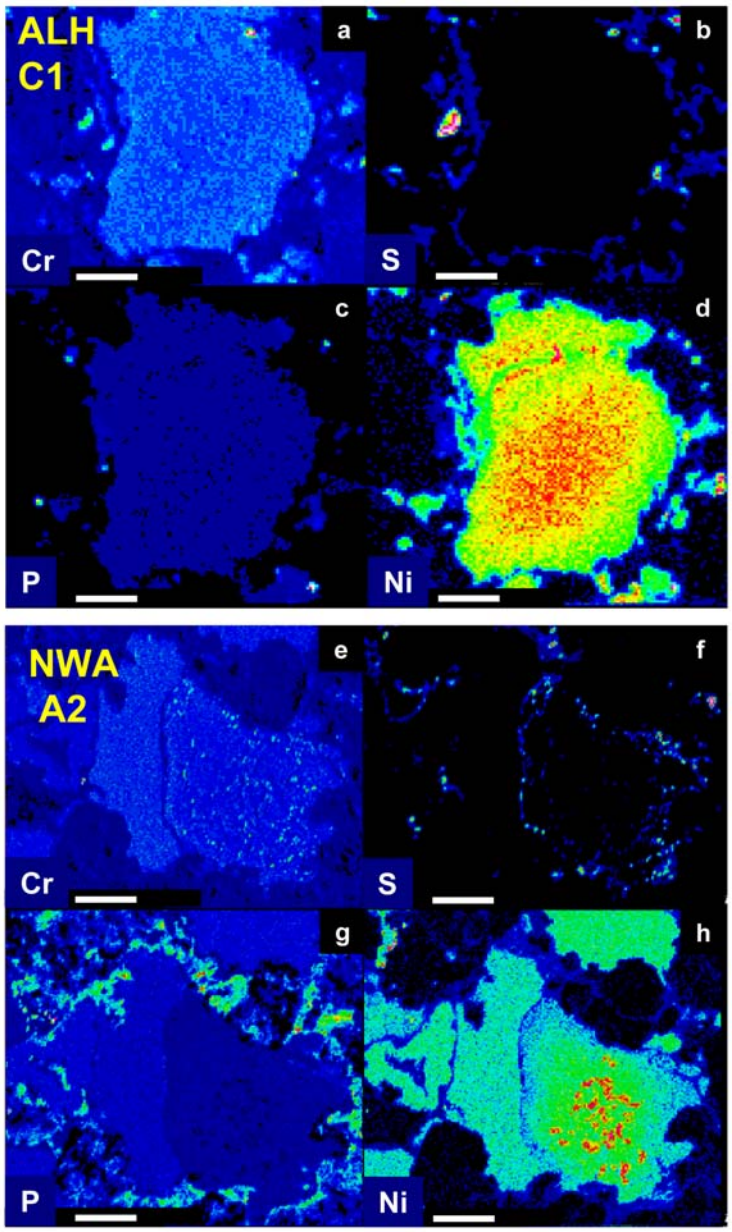

Fig. 3. Elemental X-ray scanning maps for Ni, Cr, S, and P. a–d) Zoned metal particle ALH C1. e–h) Zoned metal particle NWA A2. Ni-rich, P-poor taenite precipitates can be observed in (g) and (h). Color thermal scale: black = low element concentration, red = high element concentration.

800 K for more than 2.5 h, or taenite precipitates would have been observed in the TEM samples.

Zoned Metal with Precipitates (ZP)

The central regions of these zoned metal particles are enriched in Ni as is typical for zoned metal particles. However, the central regions also contain Ni-rich, Co- and P-poor exsolution precipitates. Figures 1c and 1d show the microstructure of two zoned condensate particles with precipitates, NWA A2 (75 × 75 μm) and PAT B2 (120 × 150 μm). Both microstructures are similar to the zoned condensate particles (Figs. 1a and 1b) in which there is an unetched region around the outside of the particle. Exsolution phases are observed in the center of particle NWA A2 and PAT B2 (Figs. 1c and 1d). Figures 6a and 6b show the variation of Fe, Ni, Co, and P along line scans across NWA A2 and PAT B2, respectively. The variation of Cr along the line scan across PAT B2 is also displayed. The overall Ni content increases from the edge of the particle to the center of the particle as is typical for a zoned condensate particle. However, the Ni gradient is no longer smooth but is

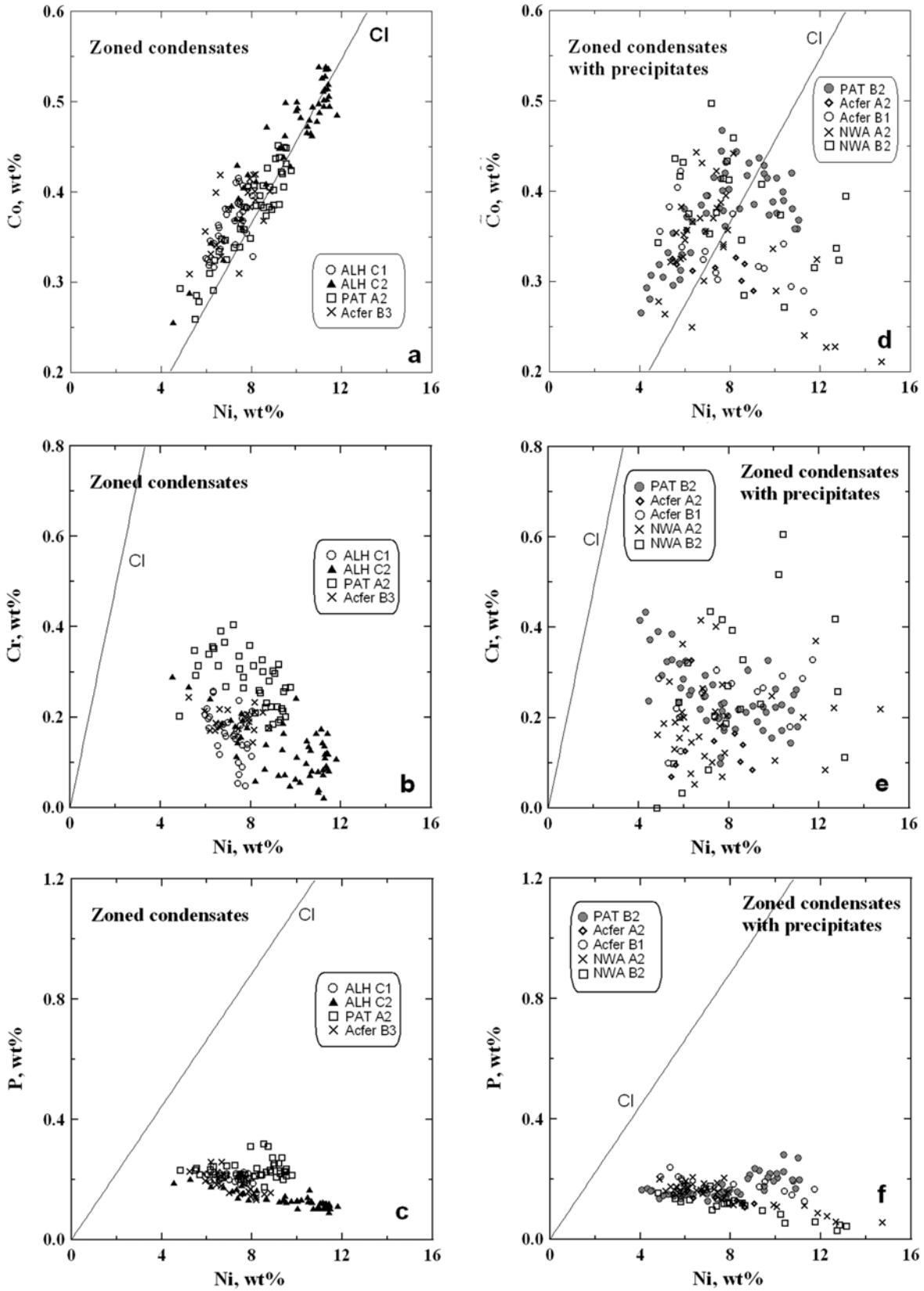

Fig. 4. Variation of (a) Co, (b) Cr, and (c) P versus Ni in four zoned metal particles. Variation of (d) Co, (e) Cr, and (f) P in five zoned condensate metal particles with precipitates. The C1 solar line is also plotted for each diagram.

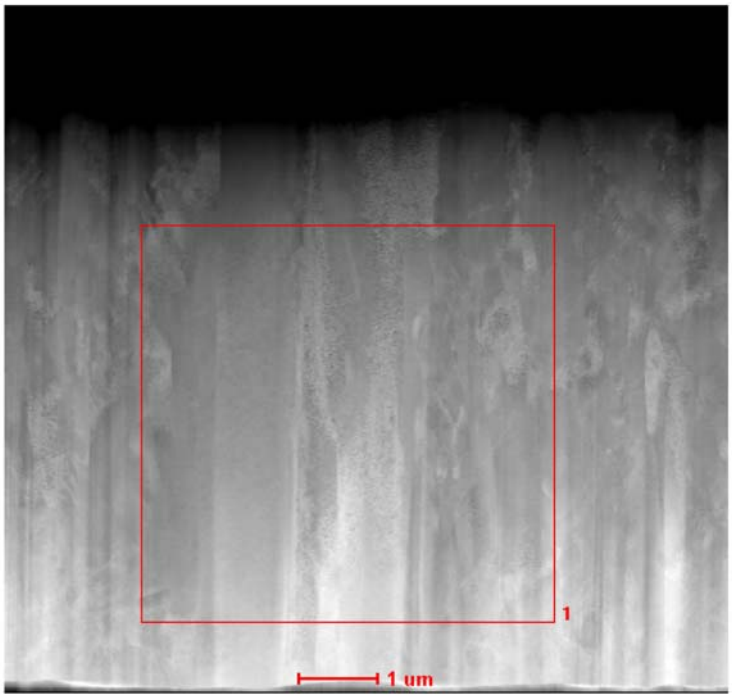

Fig. 5. STEM annular dark-field image of a TEM thin section of zoned particle ALH C1. The microstructure is lath martensite. The box identifies the 4 × 4 μm region from which an X-ray scan (128 × 128 pixels) was obtained.

interrupted by Ni-rich precipitates in the central region of the metal particles (Fig. 6). The microstructural elements in the middle of the particles are taenite precipitates as reflected by the large variations of Ni content along the Ni gradient. The Ni-rich precipitates are P- and Co-poor and the Ni-poor kamacite matrix is enriched in P and Co. Chromium does not appear to be preferentially segregated to either kamacite or the taenite precipitates. Figures 3e–h display an X-ray area map of metal particle NWA A2. The Ni-rich, P-poor taenite precipitates are observed. In addition, small (≤1 μm) Cr sulfides are observed throughout the particle. The S content of the metal, however, is 0.01–0.02 wt%. Figures 4d–f show the variation of Co, Cr, and P with Ni for five zoned metal particles with precipitates. A comparison of the composition variation diagrams of Figs. 4d–f and Figs. 4a–c (zoned metal), shows a decrease in Co content and an increase in Cr content in taenite particles at Ni contents above 8 wt%. More significantly, for Ni contents less than 8 wt%, the Co-Ni variation no longer follows the C1 solar line. In addition, Co and P decrease with increasing Ni content due to re-equilibration between the high-Ni taenite precipitates and the low-Ni kamacite matrix.

In order to obtain spatial resolution better than 1–2 μm for the composition of the submicron precipitates and surrounding matrix, FIB samples for TEM analysis were made for three zoned metal particles with precipitates, NWA B2, Acfer A2, and NWA A2. Figures 7a and 7b show the TEM section and an Ni X-ray scan of a 4 × 4 μm region of the TEM thin section of NWA B2. We observe in Fig. 7a iron, chromium-rich sulfides, <100 nm in size (dark particles), and numerous submicron Ni-rich precipitates. These precipitates contain approximately 12 wt% Ni although some contain up to 20 wt% Ni (Fig. 7b). The precipitates are surrounded by kamacite of 4–5 wt% Ni. Some precipitates, which nucleate on kamacite grain boundaries, contain 16–18 wt% Ni. We estimate particle reheating to ~950 K with the formation of high-Ni taenite followed by cooling to ~875 K in a month (Smith and Goldstein 1977). Figure 7c shows a TEM thin section of Acfer A2 which contains high-Ni precipitates about 0.5 × 0.1 to 0.2 μm in size, sulfides, and a microstructure similar to NWA B2. Ni contents of about 17 to 19 wt% are measured in the precipitates with the surrounding kamacite containing about 4.5 wt% Ni. X-ray scanning data (Fig. 7d) show that these precipitates contain as much as 20 wt% Ni. Grain boundary diffusion was observed with Ni contents in the kamacite/kamacite boundaries of 6–6.3 wt%. We estimate particle reheating to ~875 K with the formation of high-Ni taenite for approximately 2 days. Figures 8a and 8b show a lath-like structure with 50 nm chromium-rich FeS particles at kamacite-taenite interfaces in particle NWA A2. An Ni X-ray scan of the FIB section shows taenite precipitates of sizes from 1–2 μm to <200 nm (Fig. 8b). X-ray scans across submicron-size taenite particles in the thin section show taenite precipitates with a classic “M”-shaped Ni profile. Precipitation at grain boundaries and grain boundary diffusion are also observed. Figure 9 shows a submicron-size taenite particle and the Ni distribution across the 200 nm (0.2 μm) wide precipitate. Using the Ni concentration gradient in

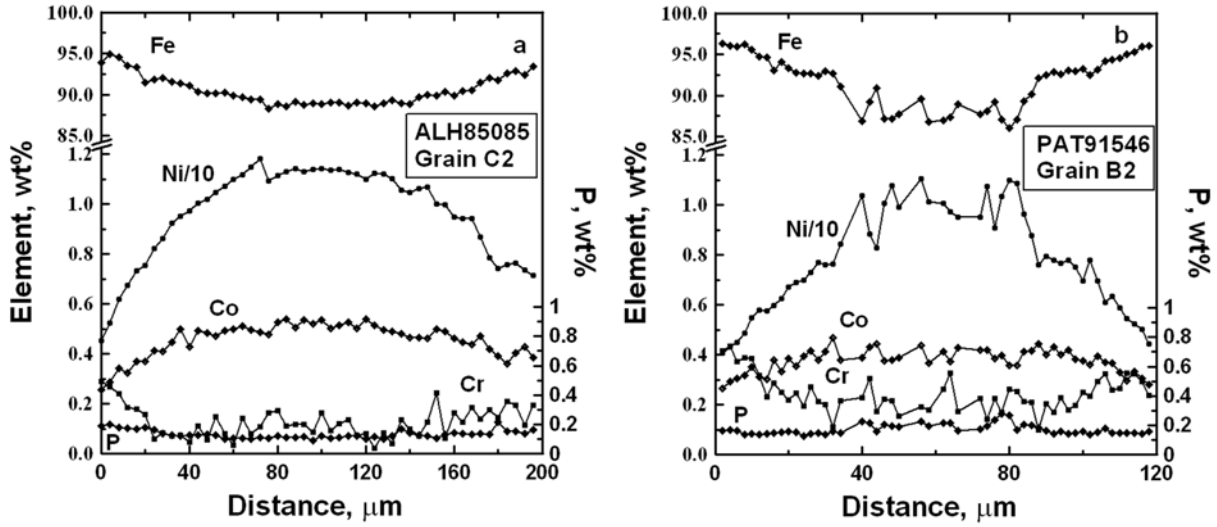

Fig. 6. a) and b) Variation of Fe, Ni, Co, and P across zoned particles with precipitates, NWA A2 and PAT B2, respectively. (The Cr variation for particle PAT B2 is also displayed.) The microstructure of these two particles is shown in Figs. 1c and 1d.

Fig. 9b, we estimate particle reheating to about 900 K for less than a week followed by cooling to below 800 K during a similar period of time (Smith and Goldstein 1977).

Unzoned Particles (UZ)

These particles are one-phase kamacite and do not contain precipitates. Figures 1c and 10a–d show the microstructure of 5 unzoned homogeneous particles. Figure 1c shows a 40 × 150 μm unzoned metal grain, NWA A2H, which has a featureless microstructure and is in intimate contact with zoned metal particle NWA A2, which contains submicron-size precipitates. Figure 10a displays a 55 × 65 μm unzoned metal grain, PAT A4, which contains grains of differing sizes. These newly formed kamacite grains are a result of a process in which metal is first mechanically deformed at low temperature, <500 K, and then reheated (recrystallization). In addition, Fig. 10b also shows two unzoned particles that are in intimate contact, 25 × 50 μm NWA A4, and 50 × 75 μm NWA A4L. Figure 10c shows a 120 × 90 μm unzoned metal grain Acfer B4 which is also recrystallized after low temperature deformation, <500 K, and contains grains of different sizes, and Fig. 10d shows a 50 × 60 μm unzoned polycrystalline metal grain, Acfer B5, with a number of 15 μm polygonal grains. Figures 11a–c show the variation of Co, Cr, and P with Ni from 10 unzoned homogeneous metal particles. These metal particles have a small variation in Ni content, 4–6 wt%, and Co contents of 0.2–0.4 wt%. The Co and Ni compositions of the metal particles parallel but do not fall on the C1 solar line. Except for particle PAT A4, which contains phosphides, the P contents of each particle are tightly clustered. The Cr content of the particles varies due partly to the presence of Cr-rich sulfides, some of which are micron-size or less. The matrix metal contains <0.01–0.02 wt% S. Particle NWA A2H has a Cr content of 0.45 ± 0.05 wt% and does not contain sulfides.

Particle NWA A4 (Fig. 10b) contains large amounts of Cr and Si: 1.3–1.6 wt% Cr, and ~3.5 wt% Si. It has a mean Co content of 0.31 wt% and a mean P content of 0.18 wt%. Particle NWA A4L (Fig. 10b) is in intimate contact with NWA A4 but only contains ~0.2 wt% Cr and <0.01 wt% Si. Si-rich grains have been observed previously in CH chondrites (Weisberg et al. 1988).

Several unzoned metal particles have been mechanically deformed below 500 K and new strain-free grains form after reheating (recrystallization) (Fig. 10). Figure 12 displays an EBSD pattern of particle Acfer B5 (Fig. 10d). The kamacite is polycrystalline and each crystal has a different crystal orientation, as shown by the different colors in the EBSD photograph (Fig. 12a) and the kamacite orientation maps (Figs. 12b–d). The EBSD photograph in Fig. 12a has a number of unindexed pixels. The lack of indexing is mainly due to our inability to carefully repolish this thin section since the sample was very thin after initial preparation for EPMA and SEM analysis.

EPMA X-ray analysis has shown that the metal particles are homogeneous in Ni at the micron level. Some precipitates have formed, Cr-rich sulfides or phosphides (e.g., particle PAT A4), but no taenite exsolution is observed. To determine if precipitates or shock structures have formed at the submicron level, we cut an FIB sample from the center of unzoned particle NWA A2H (Fig. 1c) along the direction of an EPMA trace. This particle contains 5.5 ± 0.2 wt% Ni, 0.27 ± 0.02 wt% P, 0.47 ± 0.03 wt% Co, and 0.45 ± 0.05 wt% Cr. The STEM image in Fig. 13 shows the microstructure of the particle in a 4 × 4 μm region of the thin section. A number of kamacite grains, or perhaps low-Ni martensite, are about 500 nm to 1 μm across, and are separated by grain

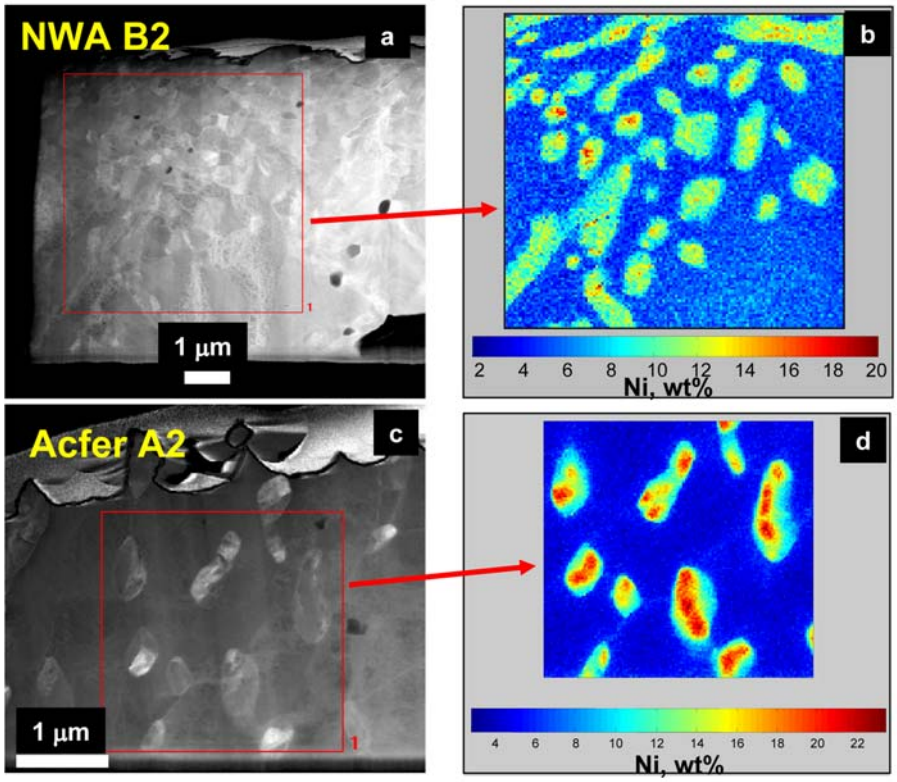

Fig. 7. Microstructures of zoned particles with precipitates: NWA B2 and Acfer A2. a) STEM annular dark-field image of the FIB section of NWA B2. b) Ni X-ray scan of a 4 × 4 µm region of the TEM thin section shown in (a). Note iron, chromium-rich sulfides, <100 nm in size (dark particles in [a]) and numerous submicron Ni-rich precipitates. c) STEM annular dark-field image of the FIB section of Acfer A2. d) Ni X-ray scan of a 2.5 × 2.5 µm region of the TEM thin section shown in (c). A color thermal scale is used. The boxes in (a) and (c) identify the regions from which the X-ray scans were obtained.

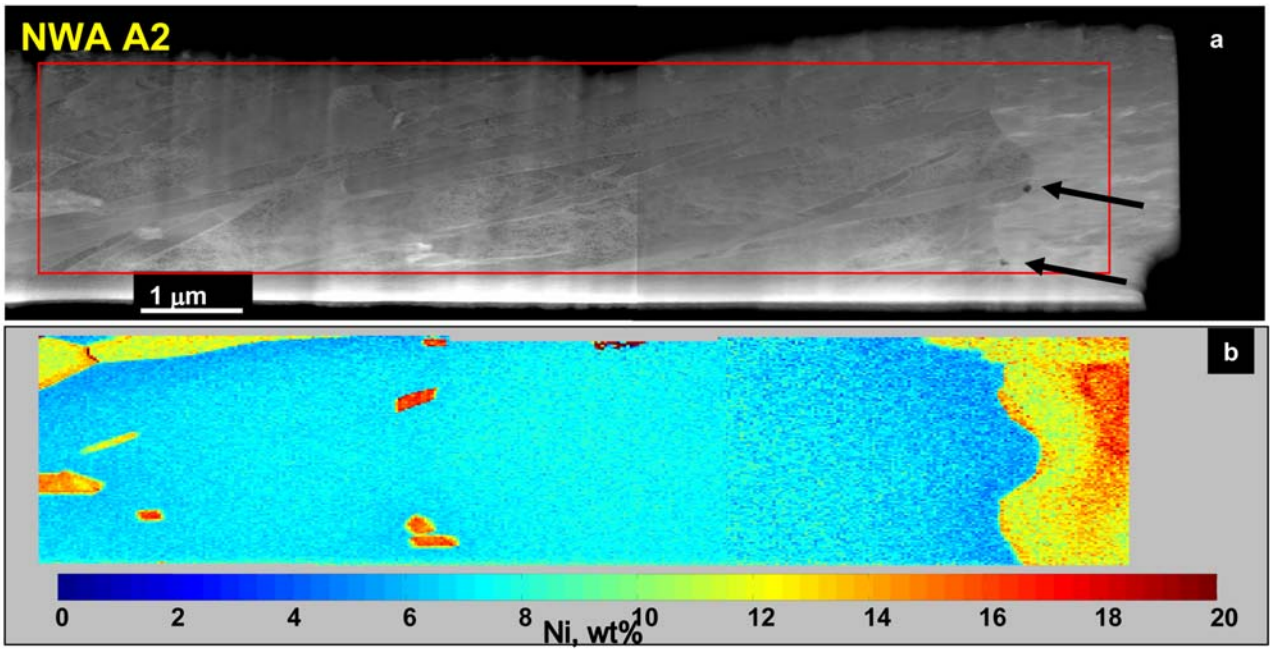

Fig. 8 a) TEM thin section of particle NWA A2 (zoned with precipitates). b) Ni X-ray scan of the TEM thin section in (a). A color thermal scale is used. A lath-like structure is observed with 50 nm chromium-rich FeS particles (arrowed) at a kamacite-taenite interface and taenite precipitates of sizes from 1–2 µm to <200 nm are observed.

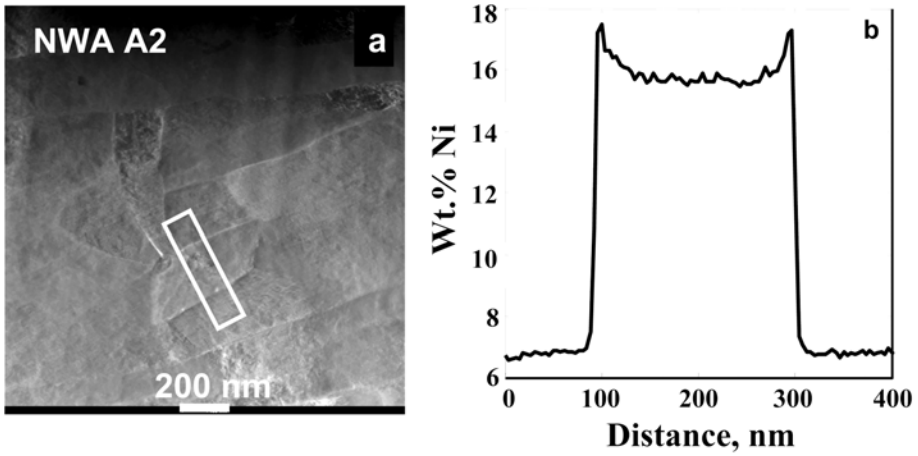

Fig. 9. a) STEM photograph of a submicron-size taenite precipitate in the TEM thin section of particle NWA A2 (Fig. 8). b) Ni distribution across the 200 nm wide precipitate shown in (a).

boundaries. These grains contain subgrains ~500 nm long by 100 nm wide, which are bent due to major plastic deformation. No precipitates are observed, using an X-ray scan with a resolution of ≥8 nm, at grain or subgrain boundaries or in the kamacite matrix of the TEM section. This particle was apparently mechanically deformed but was not reheated and/or recrystallized.

Unzoned Particles Containing Precipitates (UZP)

These metal particles do not have the regular variations in Ni, Fe, Cr, Co, etc., that are characteristic of zoned condensate particles. On the other hand, it is difficult to establish if these particles were originally unzoned (chemically homogeneous) because they contain precipitates. The microstructure of two unzoned particles containing precipitates, NWA B1B (100 × 200 μm) and Acfer A1 (100 × 120 μm) are shown in Figs. 14a and 14b, respectively. These metal particles have irregular shapes and Acfer A1 (Fig. 14b) contains recrystallized polycrystalline grains of kamacite. Both particles contain taenite precipitates throughout the microstructure. Figure 15 shows Ni, P, S, and Cr X-ray scanning pictures of NWA B1B and Acfer A1 as well as PAT E1 (60 × 80 μm) and PAT A3 (40 × 40 μm). Particle PAT E1 resides within a chondrule. All the precipitates are micron-size and Ni-rich, and extend throughout the unzoned metal particles. P is lower in the Ni-rich precipitates and higher in the surrounding kamacite (see Fig. 15, Acfer A1). Cr is segregated in taenite precipitates, some of which are >2 μm wide, in PAT A3, and also in Acfer A1. NWA B1B is low in P content (<0.01–0.03 wt%) and Acfer A1, PAT A3, and PAT E1 contain micron- and submicron-size sulfides. The metal matrix contains <0.02 wt% S. Figures 11d–f show the variation of Co, Cr, and P with Ni for five unzoned metal particles containing precipitates. Unzoned particles containing precipitates have a much greater range of Ni content than the unzoned homogeneous metal particles. Co varies inversely with Ni content, a variation which is directly opposite to the direction of the C1 line and the Co-Ni trend in zoned CH chondrite metal. Decreasing P with increasing Ni content is more pronounced than in zoned condensate metal with precipitates (Figs. 4d–f). The precipitation process involves equilibrium partitioning of Co and P, and in some cases Cr, between the low-Ni kamacite and the Ni-rich taenite precipitates.

FIB samples for TEM analysis were made for three unzoned metal particles with precipitates, PAT E1, Acfer A1, and PAT A3. FIB sections were taken from the center of the particles along the path of EPMA line analyses across the particles. The positions of the FIB samples are shown on the X-ray scanning pictures (Fig. 15). Figure 16 shows a STEM image of a portion of the FIB section from PAT E1. The X-ray image of a 4 × 4 μm region of the FIB section indicates that taenite is present at the kamacite grain boundaries. However, the Ni content varies through the grain boundary taenite as shown in Figs. 17a and 17b with a maximum of about 7.4 wt% in the center of the 1-micron-wide taenite precipitate. The kamacite-taenite border is not sharp or well defined in the X-ray image and the kamacite grain contains about 5 wt% Ni. Ni contents at the grain boundaries of other grains in the FIB section reach 12 wt%. A similar microstructure is observed in metal particle Acfer A1 in which the boundaries between kamacite and taenite are also not sharp or well defined. Figures 17c and 17d show an X-ray scan and an Ni profile across a taenite particle approximately 600 nm wide in Acfer A1. As in PAT E1, the Ni content in taenite varies with a maximum Ni content of about 7.0 wt%. The kamacite at the boundary with taenite contains about 4 wt%. A complex thermal cycle has taken place. Initially, these metal particles were heated to about 1025 K for several hours where taenite precipitates nucleated and grew. A second but brief heat treatment at higher temperatures

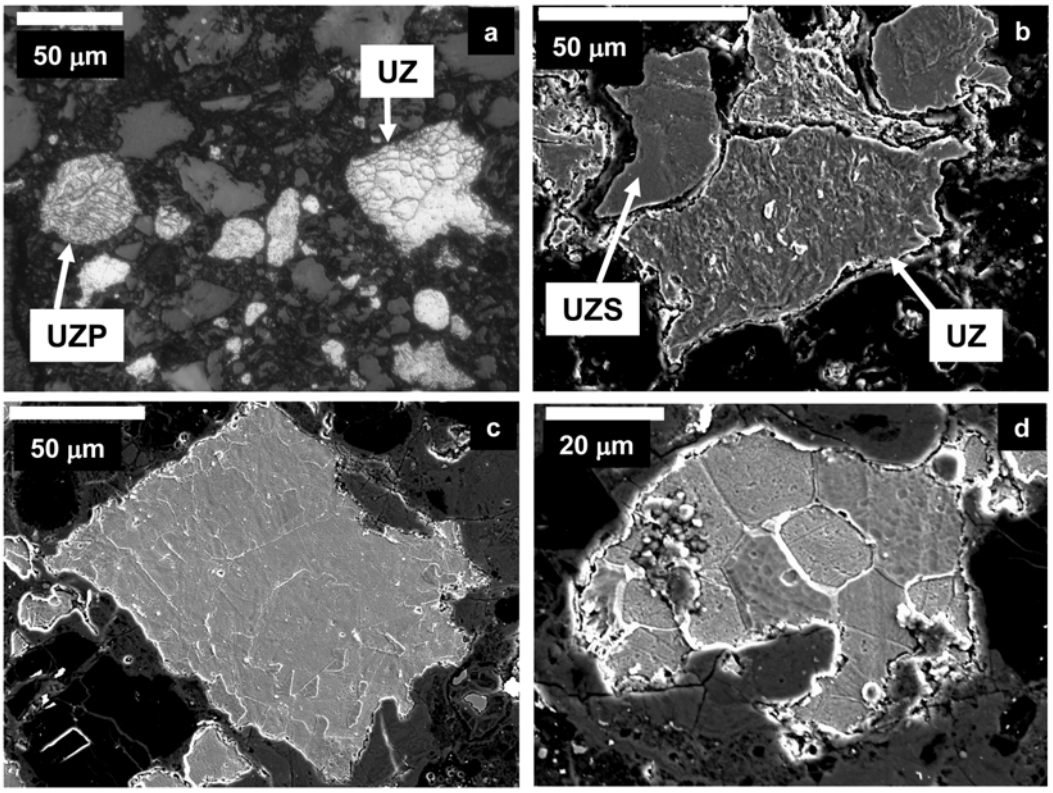

Fig. 10. Microstructures of unzoned metal particles. a) Optical photomicrograph of unzoned metal grain, PAT A4 (UZ) and unzoned metal grain, PAT A3, with precipitates (UZP). b) Secondary electron photomicrograph of two unzoned particles which are in intimate contact, NWA A4L (UZ) and NWA A4 (UZS). NWA A4 is Cr- and Si-rich. The unzoned (UZ) particle is plastically deformed as shown by the twisted grains in the microstructure. c) Secondary electron photomicrograph of unzoned metal grain Acfer B4. d) Secondary electron photomicrograph of unzoned polycrystalline metal particle, Acfer B5.

allowed for the partial dissolution of the taenite precipitates. We estimate that the metal particles were then cooled over a period of less than a day. Chromium-rich sulfides are observed in both PAT E1 and Acfer A1 metal particles. In Acfer A1, we also observed submicron particles which were Cr rich and contained V. The particles may be a sigma phase, approximately FeCr composition which forms in Fe-Ni and Ni-base superalloys in the temperature range 925–1140 K (Baker 2004).

Metal particle PAT A3 has a very different microstructure than PAT E1 and Acfer A1. Figures 16c and 16d show a region of the FIB thin section. A 2 × 2 μm X-ray scan shows a low-Ni kamacite region at the top of the scan which contains about 4.5 wt% Ni. Taenite borders the kamacite region with a varying Ni content from about 9 wt% at the kamacite/taenite border. Within the taenite there is a complex array of taenite precipitates with what appears to be swirls of Ni-rich precipitates. The taenite contains about 13 wt% Ni and the Ni-rich precipitates contain up to 30 wt% Ni. Other regions of the FIB thin section contain fine precipitates of up to 30 wt% Ni in a taenite matrix of about 8–9 wt% Ni. The development of such a complex microstructure (Figs. 16c and 16d) argues for a multistage heating/reheating process, possibly with the superposition of shock or mechanical deformation. Extensive heat treatment at temperatures around 775 K was probable in order to form fine precipitates containing ~30 wt% Ni.

High-Ni Metal Particles

A high-Ni metal grain of 50-50 Fe-Ni was observed in ALH 85085. The particle is small, 10 × 20 μm in size, and contains Co of <0.03 wt% and Cr of ~0.02 wt%. The Co content is almost an order of magnitude lower than the other four types of metal particles.

DISCUSSION

The CH metal we have studied includes particles with varying thermal histories. Metal particles with differing thermal histories and perhaps varying redox conditions during condensation appear to be attached to one another (Figs. 1c, 10b, and 14a) and it is hard to understand how the microstructures of these particles can be produced in the same physical location. Figure 18 summarizes the varying thermal histories deduced from observations in this study and by others, for the four main groups of metal particles: zoned with

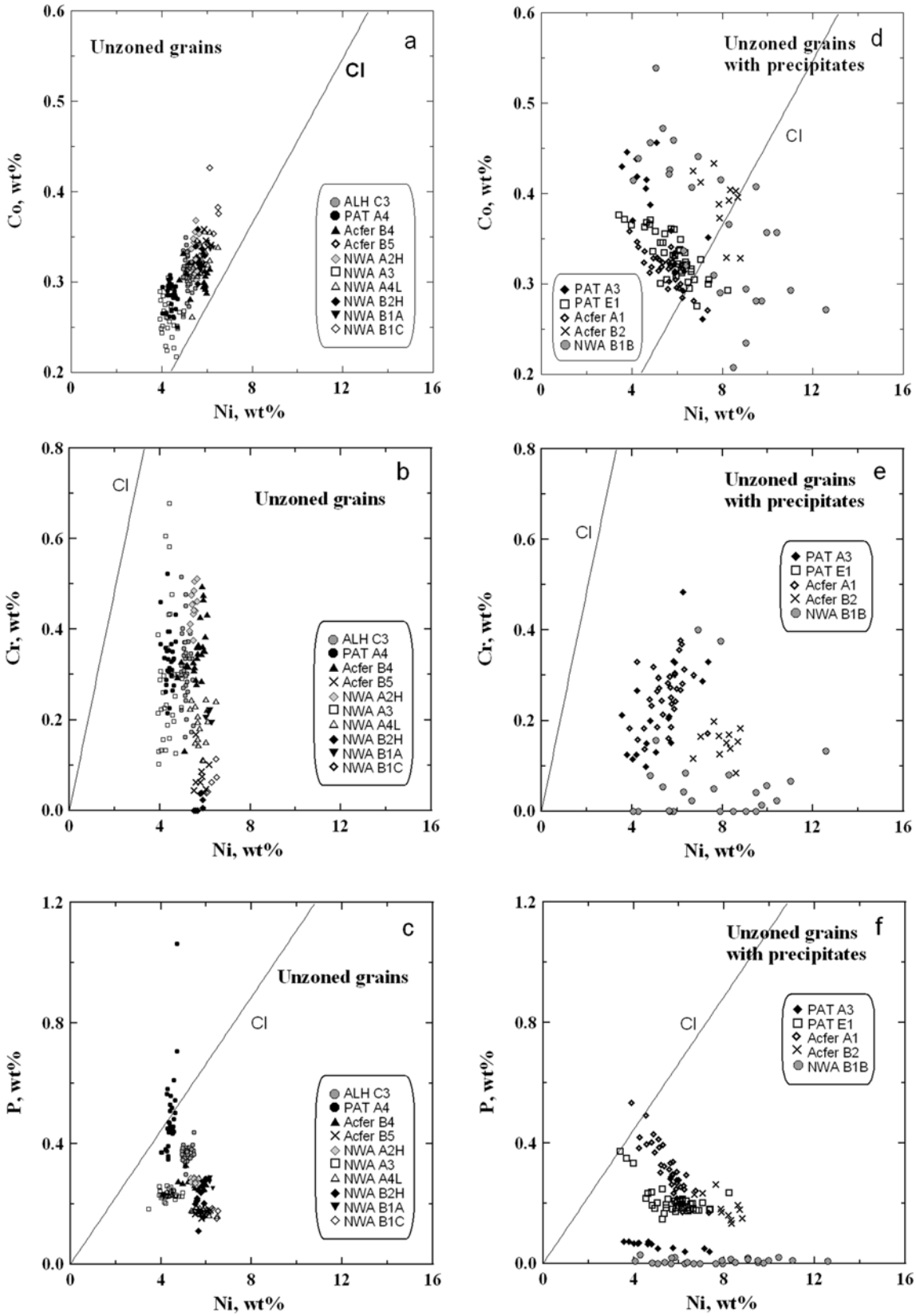

Fig. 11. Variation of (a) Co, (b) Cr, and (c) P versus Ni for ten unzoned homogeneous metal particles. Variation of (d) Co, (e) Cr, and (f) P versus Ni for five unzoned metal particles containing precipitates. The C1 solar line is also plotted for each diagram.

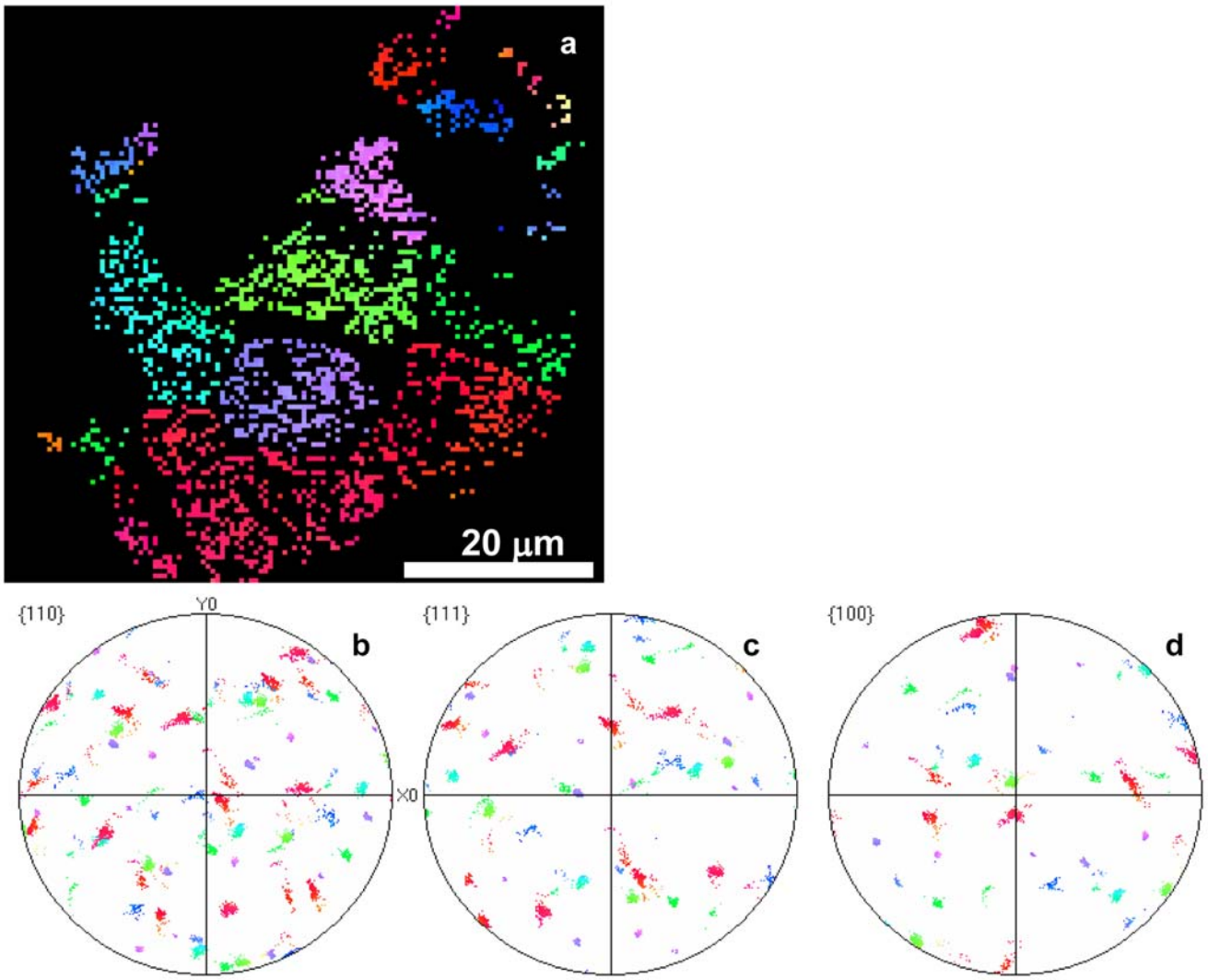

Fig. 12. a) EBSD pattern of unzoned particle Acfer B5 (Fig. 10d). b–d) Kamacite orientation maps: (b) {110}, (c) {111}, (d) {100}. The colors indicate different orientations for each kamacite crystal.

no precipitates (Z), zoned with precipitates (ZP), unzoned with no precipitates (UZ), and unzoned with precipitates (UZP). In the following section we summarize our interpretations of the thermal histories of the different particles.

Thermal Histories

One approach to understanding the diverse microstructures of the metal particles is to assume that all the metal had as its origin gas-solid condensation in the solar nebula (Meibom et al. 2000). The zoned condensates have varying Ni-Co contents (4 wt% Ni, 0.25 wt% Co to 12 wt% Ni, 0.55 wt% Co) (Fig. 4a), and formed between 1360 and ~1250 K (Campbell et al. 2005a). The unzoned homogeneous particles fall in a tight Ni-Co content cluster (4 wt% Ni, 0.2 wt% Co to 6 wt% Ni, 0.40 wt% Co) (Fig. 11a). According to Campbell and Humayun (2004), who studied trace-element compositions of unzoned CH metal, the unzoned metal particles are also condensation products. They formed at a range of temperatures that overlapped the condensation temperature of the zoned metal extending down to ~1100 K, at slow cooling rates which permitted chemical homogenization (Campbell et al. 2005a). Apparently, for the unzoned metal particles we studied, the Co-Ni variation does not exactly follow the C1 solar line.

Other mechanisms for forming the diverse microstructures of the metal particles, such as homogenizing zoned metal grains (Reisener et al. 2000), have been proposed. The varying degree of Ni zoning shown in Fig. 2 demonstrates that there is probably a continuum between the two endmember types, zoned and unzoned condensates although sectioning effects may not allow exact

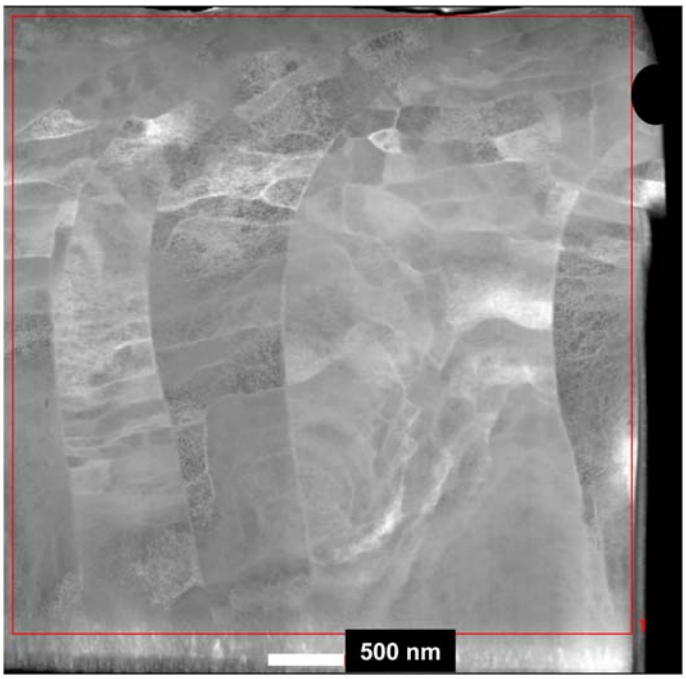

Fig. 13. STEM image of a 4 × 4 μm region of the TEM thin section from the center of unzoned particle NWA A2H along the direction of the EPMA trace shown in Fig. 1c. The kamacite grains are twisted and plastically deformed. The box identifies the region from which the X-ray scan was obtained.

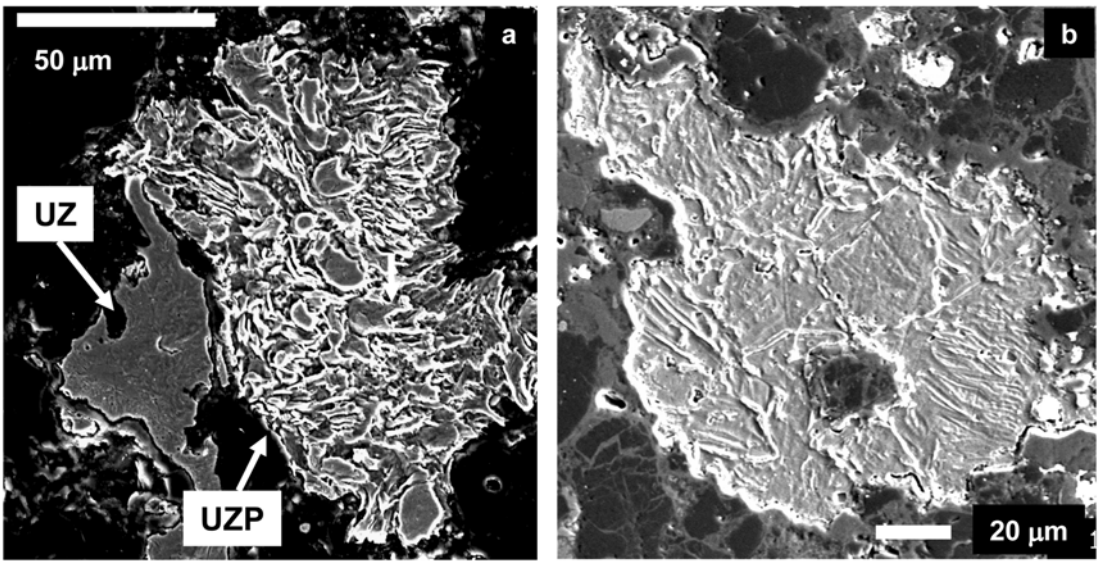

Fig. 14. Secondary electron photomicrographs of unzoned particles with precipitates (UZP). a) NWA B1B. b) Acfer A1. In (a), UZ denotes unzoned particle NWA B1A.

measurements of the maximum amount of Ni zoning. Effects of reheating and later stage precipitation make it difficult to determine the initial state of the Ni distribution in metal particles that we classify as unzoned metal particles with precipitates. In the following subsections, we discuss the implications of these thermal histories for each type of metal particle which is observed in the CH chondrites.

Zoned Condensate Metal Particles

The zoned condensate metal particles contain martensite, α_2, in the center of the metal particle, which is surrounded by a featureless region of kamacite, α. No precipitates (e.g., taenite, γ, or Cr-rich sulfides) 4 nm or larger are observed. The Ni (4–12 wt%) and P contents (0.1–0.3 wt%) of the zoned condensates are such that slow cooling

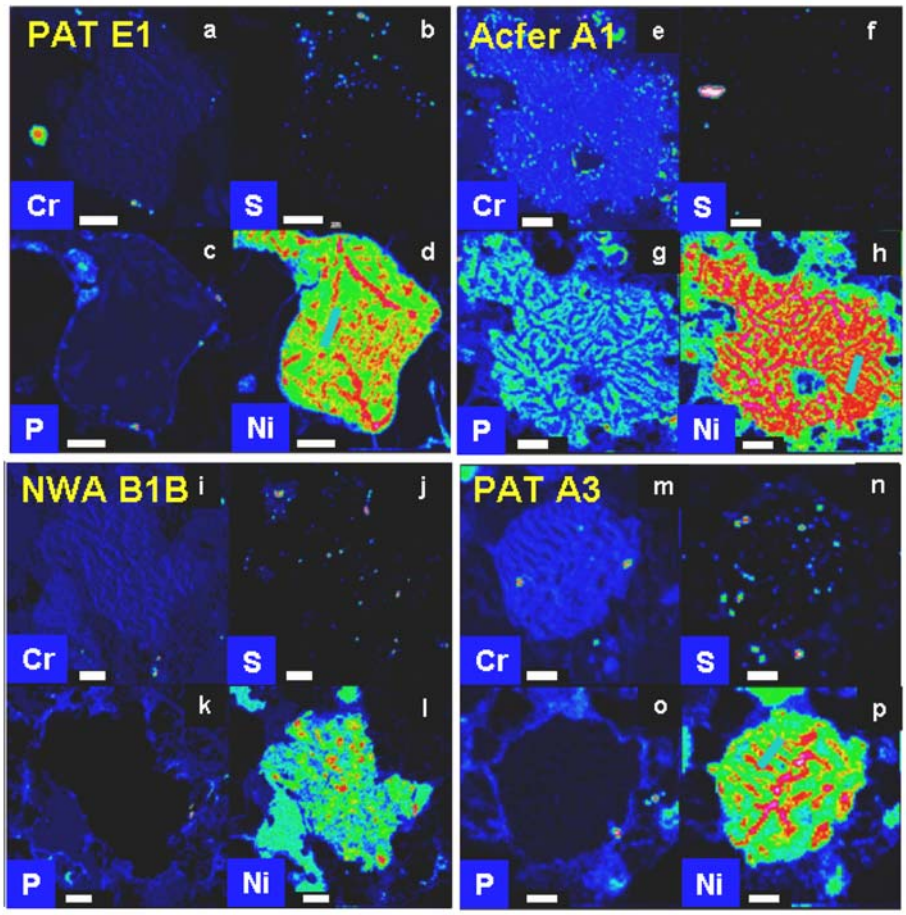

Fig. 15. Elemental X-ray scanning maps for Ni, Cr, S, and P across unzoned particles containing precipitates (UZP). a–d) PAT E1. e–h) Acfer A1. i–l) NWA B1B. m–p) PAT A3. (i–l) also show UZ particle NWA B1A (see Fig. 14a). The position of the FIB samples is shown by the blue bars in (d), (h), and (p). Color thermal scale: black = low element concentration, red = high element concentration. The scale bars are 20 μm, except for PAT A3, which has a scale bar of 10 μm.

after condensation will produce a Widmanstätten pattern by the mechanism $\gamma \rightarrow \alpha_2 + \gamma \rightarrow \alpha + \gamma$ according to Yang and Goldstein (2005). The presence of martensite, α_2, and the corresponding lack of a Widmanstätten pattern or α-kamacite precipitates on grain boundaries in zoned condensate particles argues for fast cooling, of the order of hours or days, in the temperature range of 1000 K or below as shown experimentally by Reisener and Goldstein (2003) (Fig. 18). We have not observed sulfides in zoned condensate metal particles and S contents are <0.01 wt%. Therefore it is unlikely that S was incorporated during the condensation process.

Unzoned Condensate Metal Particles

The unzoned condensate metal particles are one phase kamacite. Several of the kamacite particles are polycrystalline (Figs. 10a, 10c, and 10d), several others contain Cr-rich sulfides, and several of the particles have been plastically deformed (Figs. 10b and 13). The polycrystallinity of many of these metal particles indicates a period of reheating after some degree of prior plastic deformation below 500 K. EBSD analysis of recrystallized particle Acfer B5 (Figs. 10d and 12) shows that the reheating cycle formed individual kamacite grains of differing orientations. Recrystallization temperatures were below ~900 K or taenite would form on reheating the unzoned condensate particles into the $\alpha + \gamma$ phase field (Fig. 18). Unzoned condensate particle PAT A4 contains 4.2 wt% Ni and a high P content (0.5 ± 0.1 wt%) and the microstructure of this particle contains recrystallized grains and phosphides (Ph). The formation of phosphides is consistent with reheating to a recrystallization temperature of 800–900 K where the bulk composition of the metal particle is in the α + Ph phase field of the Fe-Ni-P phase diagram (Romig and Goldstein 1980) (Fig. 18).

Apparently most of the unzoned condensate particles have been plastically deformed at one time or another. It is not clear when this deformation occurred, during condensation or before incorporation of the metal particles into the final CH chondrite breccia (Fig. 18). With Ni contents <5.5 wt% and P contents of more than about

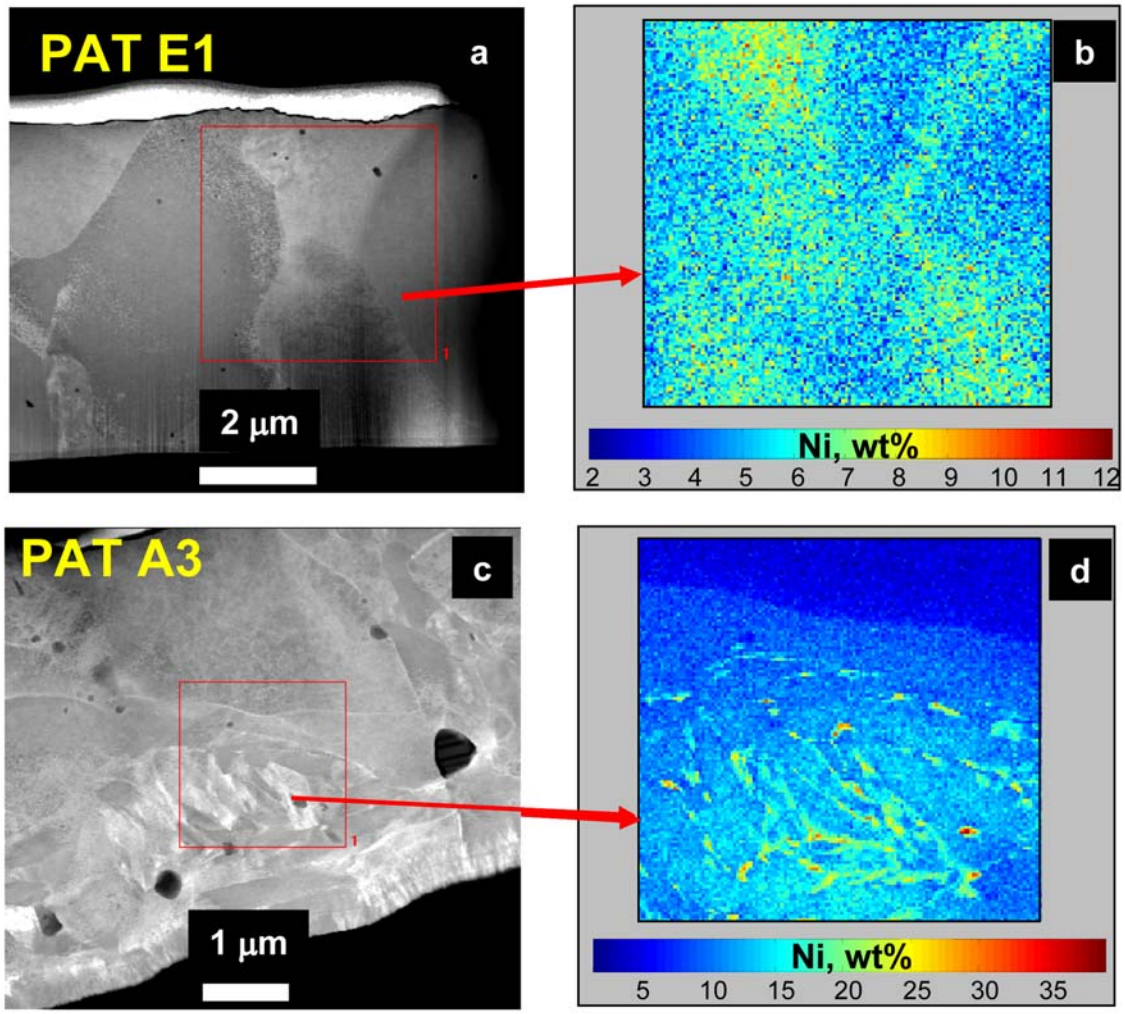

Fig. 16. Unzoned particles with precipitates. a) STEM image of a portion of the FIB section from PAT E1. b) Ni X-ray image of a 4 × 4 μm region, outlined in (a) of the FIB section. c) STEM image of a portion of the FIB section from PAT A3. d) Ni X-ray image of a 2 × 2 μm region, outlined in (c) of the FIB section.

0.1 wt%, it would be expected that kamacite would form by a massive transformation upon cooling (Yang and Goldstein 2005). Unzoned metal particles with Ni contents from 5.5 to 6.5 wt% and P contents up to 0.3 wt% (Fig. 11) would form a Widmanstätten pattern or α-kamacite precipitates on grain boundaries unless fast cooling, of the order of hours or days, took place in the temperature range of 1000 K or below (Reisener and Goldstein 2003).

If the Ni-Co composition of the unzoned metal particles varied initially, reheating to temperatures of over 1300 K for time periods exceeding a week would be necessary to homogenize the Ni and Co. Slow cooling from these high temperatures would cause kamacite to form as a Widmanstätten pattern or as precipitates along grain boundaries for particles exceeding 5.5 wt% Ni. Fast cooling from these temperatures would be necessary to produce the martensite, α_2, structure which is observed in several metal particles. Reheating to these high temperatures (>1300 K) would require not only fast cooling after homogenization, but subsequent plastic deformation and another reheating cycle to form the recrystallized grains. We argue that this complicated thermal history is unlikely. Therefore, it is probable that the chemically homogeneous metal particles formed during condensation and were cooled rapidly, during which time some particles were plastically deformed. In some cases, reheating and recrystallization at about 800 to 900 K for a short period of time (1 hour to a day) took place after deformation (see Fig. 18).

It is important to note that the Co-Ni distribution of the zoned and unzoned grains form a continuous grouping along the C1 solar variation line (compare Figs. 4a and 11a) although the spread of Co and Ni within individual grains is very different in zoned versus unzoned grains. The unzoned grains fall at lower Ni and Co contents than the zoned grains

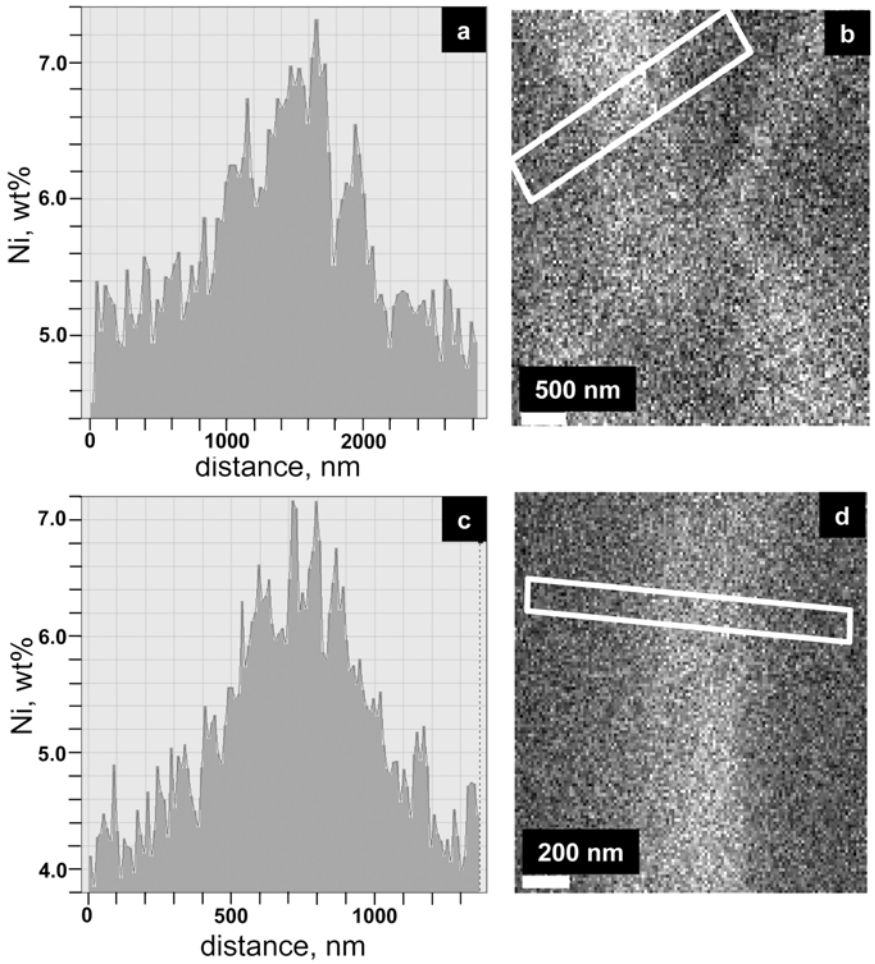

Fig. 17. a) Variation of Ni through a grain boundary high-Ni precipitate in PAT E1, an unzoned metal particle with precipitates. b) Ni X-ray image of a 4 × 4 μm region of the FIB section (Fig. 16b) showing the position of the Ni profile in (a). c) Variation of Ni through a grain boundary high Ni region approximately 600 nm wide in Acfer A1, an unzoned metal particle with precipitates. d) Ni X-ray image of a 1.5 × 1.5 μm region of the FIB section showing the position of the Ni profile in c).

and may be considered as lower temperature condensates. Campbell and Humayun (2004) also observed a positive Ni-Co correlation for zoned and unzoned metal grains from two CH chondrites with a calculated condensation trajectory for a gas of solar composition at a pressure of 10^{-4} bars. In general, the unzoned grains we have studied have lower Ni contents than those given by the C1 solar line. The reason for this behavior may be due to an inefficient fractional condensation process, in which a small portion of the condensable fraction of the gas actually condenses at a given temperature (Petaev et al. 2003), and to the diffusion process which plays a significant role in the establishment of the composition profiles (Meibom et al. 2001; Petaev et al. 2003; Campbell et al. 2005a). However, Righter et al. (2005) have shown experimentally that there is no difference in diffusion coefficients for Ni and Co at 1150 °C. Therefore, we conclude that it is probable that diffusion of Ni and Co in single crystal taenite will not measurably fractionate the Ni/Co ratio.

Zoned Condensate Metal Particles

The zoned condensate metal particles with precipitates have phases of exsolved Ni-rich taenite in the central regions of the particles. The central regions of these particles extend from a Ni content of 7–8 wt% to ~10 wt% and in some cases to >12 wt% (Figs. 2 and 6). In addition, small Cr-rich sulfides are observed in the particles. EPMA analyses show that P and Co have re-equilibrated and are depleted in Ni-rich taenite and enriched in the Ni-depleted matrix kamacite. Detailed TEM X-ray analysis indicates that the taenite precipitates may contain 12 to as much as 20 wt% Ni and the kamacite about 5 wt% Ni (Fig. 7b). These Ni compositions are consistent with heat treatments up to temperatures of ~950 K, according to the Fe-Ni-P phase diagram (Romig and Goldstein 1980), and for periods of approximately two days to a week, followed by cooling to below ~800 K, during the same period of time (Fig. 18) using the methodology of Smith and Goldstein (1977). The reheating temperatures are the same as those for many of the unzoned metal particles

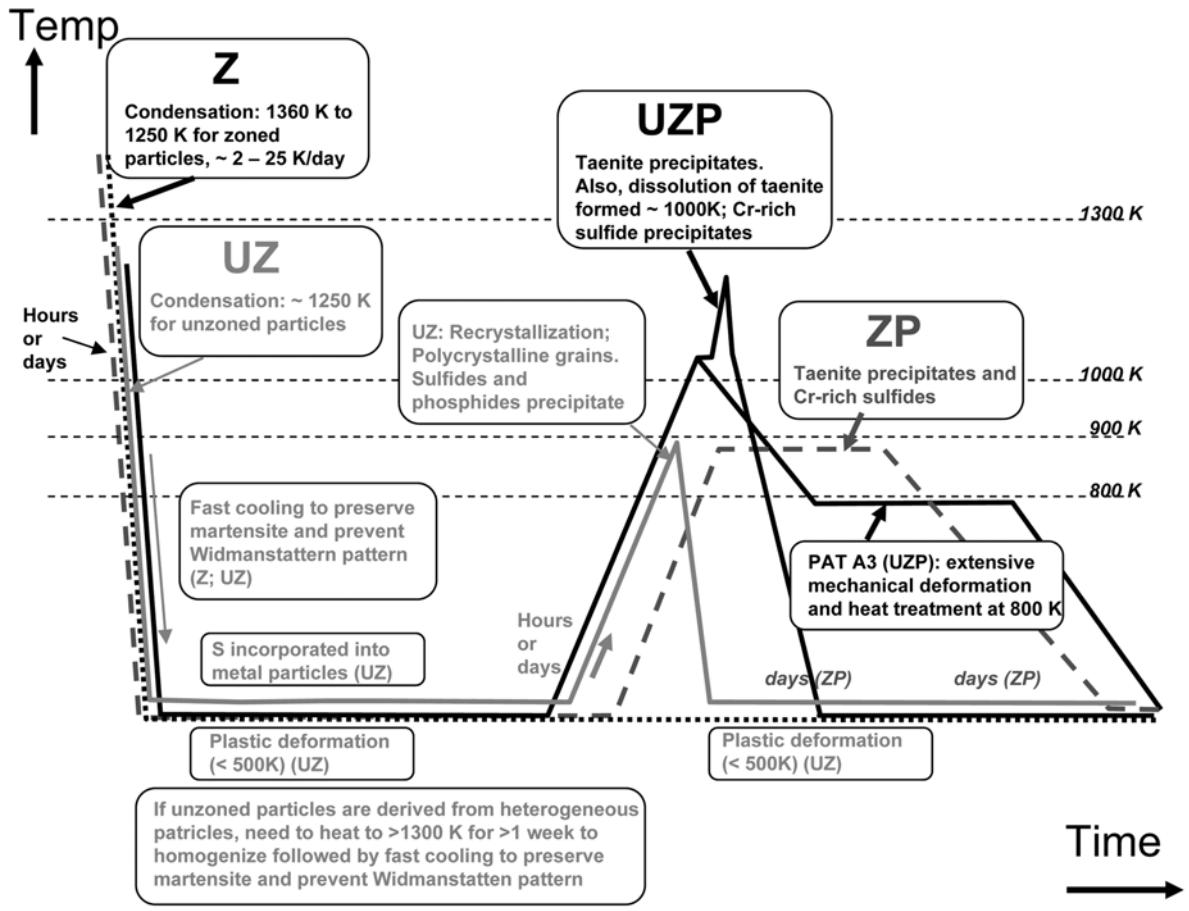

Fig. 18. Summary of the thermal histories of the four main groups of metal particles. Z = zoned, ZP = zoned with precipitates, UZ = unzoned, and UZP = unzoned with precipitates.

(~800–900 K) to as high as 950 K. The major difference in the microstructure, taenite precipitates versus recrystallized grains, is due in part to the much higher Ni content of the central regions of the zoned condensate particles.

Chromium-rich sulfides have been observed in the metal particles including the zoned condensate particles which contain precipitates. The presence of small Cr-rich sulfides, particularly in the TEM sections, can be explained by the nucleation of sulfides from S supersaturated metal when heat treated at 800–900 K as shown experimentally for the Fe-Ni-S system (Ma et al. 1998). The observation that the zoned condensate particles do not contain S argues that S is not incorporated into metal during the condensation process. Therefore the probable source of the S in the zoned condensate metal particles with precipitates is the S-rich regions which surround the zoned metal particles (see Figs. 3 and 15). Some S was incorporated into the metal during heat treatment.

Unzoned Metal Particles with Precipitates

The unzoned metal particles with precipitates have phases of exsolved Ni-rich taenite (Figs. 14 and 15). These particles have a much greater range of Ni than the unzoned metal particles (compare Figs. 11a and 11d). EPMA analyses show that P, Co, and Cr have re-equilibrated. P and Co are depleted in Ni-rich taenite and enriched in the Ni-depleted matrix kamacite as observed in the Fe-Ni-P and Fe-Ni-Co systems (Romig and Goldstein 1980; Widge and Goldstein 1977). Cr is enriched in taenite and depleted in kamacite in particle PAT A3. This redistribution in Cr is not consistent with tie lines in the Fe-Ni-Cr system (Vander Voort 1992). TEM X-ray data show that two of the unzoned metal particles with precipitates have taenite particles that have been heat-treated to temperatures as high as 1025 K to form taenite precipitates and briefly to higher temperatures where dissolution of taenite has taken place (Figs. 16 and 17). Chromium-rich sulfides are most likely formed from S supersaturated metal heat-treated at higher temperatures. The sulfur is probably incorporated in the unzoned metal during low-temperature condensation of the unzoned metal particles: S starts to condense at 674 K during equilibrium condensation from a gas of solar composition (Lauretta et al. 1996). The source of the S in the unzoned metal particles may also come from the S-rich regions which surround the zoned metal particles (see Figs. 3 and 15) during the heat-treatment cycle.

Cr- and V-rich submicron particles found in Acfer A1 may be sigma phase formed in Fe-Ni alloys during heat treatment at 925–1140 K (Baker 2004). Metal particle PAT A3 underwent a very complex heat treatment in which there was superposition of shock or mechanical deformation (Figs. 16c and 16d). The shock or mechanical deformation may have been present before heat treatment as observed in the unzoned metal particles. In this particle an extensive heat treatment at around 775 K appears to have taken place forming fine precipitates with high Ni contents (Fig. 17). Although both zoned and unzoned metal particles have precipitates of Ni-rich taenite, the heat-treatment temperatures are different. The Co, Cr, and P versus Ni variations are different as well due, in part, to the different distribution of these elements between the zoned and unzoned metal particles before reheating.

One Ni-rich metal particle was observed in ALH 85085. Nickel-rich metal particles have been described previously by Meibom et al. (1999b). These authors propose that the Ni-rich metal particles form in more oxidizing conditions, a part of variable redox conditions. We have also observed one high-Cr and high-Si unzoned metal particle, NWA A4 (Fig. 10b), out of the 24 metal particles we studied. This particle contains large amounts of Cr and Si (average 1.3 wt% Cr, and 3.6 wt% Si). There is, however, no microstructural difference between this particle and other unzoned metal particles. One high-Cr and high-Si particle has also been observed in ALH 85085 by Weisberg et al. (1988) (~2.5% of the sample of metal particles) along with two high-Si particles. Weisberg et al. (1988) speculated that Si-bearing metal condensed along with other metal but may have resulted from local fluctuations of gas pressure during condensation. Meibom et al. (1999b) found that equilibrium condensation calculations of Si concentrations in metal are only in agreement with measured Si data at a total pressure of 10^{-4} bars. Together, the Ni-rich and Si-rich particles show either that redox conditions and pressure conditions in the CH formation region fluctuated, or that some grains from other regions of the nebula were mixed with metal formed in the localized CH region.

Origin of Metal in CH Chondrites

We have studied the microstructure and microchemistry of 24 metal particles in detail. Although this number of particles is not statistically significant, it appears that there are few obvious differences in the nature of the metal particles between the four CH chondrites. ALH 85085 was not represented among the zoned and unzoned metal particles with precipitates that we analyzed, although these types of particles were present in the meteorite. We also see little difference between the two types of CH chondrite, the ALH 85085–like CH chondrites (ALH 85085 and PAT 91546) and the Acfer 182–like CH chondrites (Acfer 214 and NWA 739). Overall, it appears that we can treat the CH chondrites as a single group in which metal shows similar properties.

The CB chondrites have even more metal (50–70% by volume) than the CH chondrites. The meteorites in subgroup CB_b contain three kinds of metal: zoned, unzoned, and large metal-sulfide aggregates (Weisberg et al. 2001). Major and trace elements have also been measured in the zoned and unzoned metal particles of CBb chondrites (Campbell et al. 2005a; Campbell et al. 2005b). A condensation origin is inferred for both types of metal. The CB_b metal appears to have formed by a process very similar to that of the CH chondrites although the CB_b metal has fewer particles which are zoned with precipitates. Presumably CB_b metal particles experienced even less thermal alteration following their formation (Campbell et al. 2005b).

Our data are consistent with previous studies of CH metal that have described the four main types of particles we discuss: zoned metal, zoned metal with precipitates, unzoned metal, and unzoned metal with precipitates (Meibom et al. 1999a; Campbell and Humayun 2004; Meibom et al. 1999b). The consensus of most metal studies is that zoned and unzoned condensates formed by condensation from the gas on time scales of several days, and that some grains from both of these groups were later reheated, producing precipitates. While in broad agreement, we are able to add significantly more detail to this history. We have shown that both zoned and unzoned particles with no precipitates must have continued their fast cooling paths to temperatures below 500 K in order to preserve martensite and prevent formation of the Widmanstätten pattern and/or α-kamacite on a scale of nanometers. Also, since no sulfur was incorporated into zoned particles, we know that condensation was effectively closed at a temperature around 700 K. We are unable to determine whether S was originally included in the unzoned particles. We see evidence for at least one reheating episode in several particles, but different temperature-time profiles for different grains (Fig. 18). Precipitates grew in unzoned grains that were reheated to a peak temperature around 900 K and in zoned particles with high-Ni cores at temperatures between 800 and 900 K. Taenite precipitates would be observed in the TEM samples if zoned metal was reheated to 1000 K for more than 1 s, 900 K for more than 1 min, or 800 K for more than 2.5 h.

One of the particles we examined, PAT E1, is located within a type I porphyritic olivine chondrule. It is an unzoned particle that contains precipitates, and shows evidence for dissolution of taenite at >1000 K. We might reconcile this thermal history with its location inside a chondrule by the following scenario: first it was formed as a condensate, then it was incorporated into the chondrule precursor assemblage, and finally it was reheated during chondrule formation. We might expect the metal to have melted during chondrule formation. Without the presence of sulfide, however, the metal melting temperature would exceed 1750 K. Hence, the metal particle may have survived chondrule formation as a relict grain, and taenite dissolution could have taken place

during chondrule formation. On the other hand, the metal particle could have been an unzoned grain formed during chondrule formation, then reheated as a particle within the chondrule in a later event. It is possible that other grains with similar properties could have been incorporated in chondrules at some time, and later released, when chondrules were broken apart during impact events.

The best scenario to explain all these microchemistry and metallographic observations is that condensation produced zoned and unzoned metal particles in a process in which grain growth and cooling took place on a time scale of days. At a later time, many but not all of these particles were reheated to 800–1000 K. We do not know the time interval between condensation and reheating. Brief time scales, on the order of days, for these reheating episodes indicate that this could be the result of impact heating on a parent body. The final assemblages of CH chondrites that are preserved as meteorites are breccias that were not assembled until after impact heating was complete. Brecciation juxtaposed material that has been subjected to reheating and material that escaped reheating. Evidence for mechanical deformation that postdates the reheating events is consistent with this scenario.

The two-stage thermal history we deduce for metal grains in CH chondrites must be reconciled with that of the silicate components in the same chondrites. Hezel et al. (2003) also deduced a two-stage thermal history for silica-bearing components in Acfer 182. However, the temperatures of the reheating event recorded by these objects are significantly higher than those recorded by the metals, greater than 1968 K, and the subsequent cooling rates are very rapid, some objects being essentially quenched. These thermal profiles are more consistent with the type of transient heating event associated with chondrule formation than they are with the reheating event to ~1000 K, and cooling rates over a period of days, recorded by metal grains. The silica-rich objects and the metal appear to record entirely different secondary heating events.

Acknowledgments–We thank Dr. Jijin Yang (University of Massachusetts) for discussions about metal thermal history, Mr. Michael Rye (Sandia) for assistance with the FIB samples, and Mr. M. N. Spilde (UNM) for assistance with the electron microprobe. Dr. Adrian Brearley (UNM) kindly supplied demountable TEM sections. Reviews by A. Meibom, A. J. Campbell, and D. Hezel helped to improve the paper. Financial support from NASA through grants NNG05GK84G, NAG5-9463, and NNG06GF73G are acknowledged. Sandia is a multiprogram laboratory operated by Sandia Corporation, a Lockheed Martin Company, for the U.S. Department of Energy's National Nuclear Security Administration under contract DE-AC0494AL85000. SEM and EPMA work was carried out in the Electron Microbeam Analysis Facility, Department of Earth and Planetary Sciences and Institute of Meteoritics, University of New Mexico.

Editorial Handling—Dr. Christine Floss

REFERENCES

Baker H., editor. 2004. *Alloy phase diagrams.* ASM Handbook, vol. 3. Materials Park, Ohio: ASM International. 344 p.

Bischoff A., Palme H., Schultz L., Weber D., Weber H. S., and Spettel B. 1993. Acfer 182 and paired samples, an iron-rich carbonaceous chondrite: Similarities with ALH 85085 and relationship to CR chondrites. *Geochimica et Cosmochimica Acta* 57:2631–2648.

Campbell A. J. and Humayun M. 2004. Formation of metal in the CH chondrites ALH 85085 and PCA 91467. *Geochimica et Cosmochimica Acta* 68:3409–3422.

Campbell A. J., Zanda B., Perron C., Meibom A., and Petaev M. I. 2005a. Origin and thermal history of Fe-Ni metal in primitive chondrites. In *Chondrites and the protoplanetary disk*, edited by Krot A. N., Scott E. R. D., and Reipurth B. ASP Conference Series, vol. 341. San Francisco: Astronomical Society of the Pacific. pp. 407–431.

Campbell A. J., Humayun M., and Weisberg M. K. 2005b. Compositions of unzoned and zoned metal in the CB_b chondrites Hammadah al Hamra 237 and Queen Alexandra Range 94627. *Meteoritics & Planetary Science* 40:1131–1148.

Cliff G. and Lorimer G. W. 1975 The quantitative analyses of thin specimens. *Journal of Microscopy* 103:203–207.

Grossman J. N., Rubin A. E., and MacPherson G. J. 1988. ALH 85085: A unique volatile-poor carbonaceous chondrite with possible implications for nebular fractionation processes. *Earth and Planetary Science Letters* 91:33–54.

Hezel D. C., Palme H., Brenker F. E., and Nasdala L. 2003. Evidence for fractional condensation and reprocessing at high temperatures in CH chondrites. *Meteoritics & Planetary Science* 38:1199–1215.

Jones R. H., Guan Y., Leshin L. A., Larsen T., and Sharp Z. D. 2005. Oxygen isotope distribution in NWA 739, a CH chondrite with affinities to Acfer 182 (abstract #1813). 36th Lunar and Planetary Science Conference. CD-ROM.

Keenan M. R. and Kotula P. G. 2003. Apparatus and system for multivariate spectral analysis. U.S. Patent #6,584,413, filed June 1, 2001, and issued June 24, 2003.

Keenan M. R. and Kotula P. G. 2004. Method of multivariate spectral analysis. U.S. Patent #6,675,106, filed June 1, 2001, and issued January 6, 2004.

Kotula P. G., Keenan M. R., and Michael J. R. 2003. Automated analysis of EDS spectral images in the SEM: A powerful new microanalysis technique. *Microscopy and Microanalysis* 9:1–17.

Kotula P. G. and Keenan M. R. 2006. Application of multivariate statistical analysis to STEM X-ray spectral images: Interfacial analysis in microelectronics. *Microscopy and Microanalysis* 12: 538–544.

Krot A. N., Meibom A., Russell S. S., Alexander C. M. O'D., Jeffries T. E., and Keil K. 2001. A new astrophysical model for chondrule formation. *Science* 291:1776–1779.

Krot A. N., Meibom A., Weisberg M. K., and Keil K. 2002. The CR chondrite clan: Implications for early solar system processes. *Meteoritics & Planetary Science* 37:1451–1490.

Lauretta D. S., Kremser D. K., and Fegley B. 1996. The rate of iron sulfide formation in the solar nebula. *Icarus* 122:288–315.

Leroux H. and Perron C. 2001. Microstructure of Fe-Ni metal in the Bencubbin and Hammadah al Hamra 237 meteorites (abstract). *Meteoritics & Planetary Science* 36:A113.

Ma L., Williams D. B., and Goldstein J. I. 1998. Determination of the Fe-rich portion of the Fe-Ni-S phase diagram. *Journal of Phase Equilibria* 19:299–309.

Meibom A., Petaev M. I., Krot A. N., Wood J. A., and Keil K. 1999a. Primitive FeNi metal grains in CH carbonaceous chondrites formed by condensation from a gas of solar composition. *Journal of Geophysical Research* 104:22,053–22,059.

Meibom A., Krot A. N., Petaev M. I., Wilson L., Reisener R., Goldstein J. I., Norman M., Campbell A. J., Bennett V., Nuth J., Wasilewski P., Bland P., Hough R. M., Trimby P., and Keil K. 1999b. Metal condensates in CH and Bencubbin-like chondrites: Evidence for localized nebula heating events and variations in gas composition (abstract). *Meteoritics & Planetary Science* 34: A80–81.

Meibom A., Desch S. J., Krot A. N., Cuzzi J. N., Petaev M. I., Wilson L., and Keil K. 2000. Large-scale thermal events in the solar nebula: Evidence from Fe,Ni metal grains in primitive meteorites. *Science* 288:839–841.

Meibom A., Petaev M. I., Krot A. N., Keil K., and Wood J. A. 2001. Growth mechanism and additional constraints on FeNi metal condensation in the solar nebula. *Journal of Geophysical Research* 106:32,797–32,801.

Petaev M. I., Wood J. A., Meibom A., Krot A. N., and Keil K. 2003. The ZONMET thermodynamic and kinetic model of metal condensation in the solar nebula. *Geochimica et Cosmochimica Acta* 67:1737–1751.

Reisener R. J. and Goldstein J. I. 2003. Ordinary chondrite metallography: Part 1, Fe-Ni taenite cooling experiments. *Meteoritics & Planetary Science* 38:1669–1678.

Reisener R. J., Meibom A., Krot A. N., Goldstein J. I., and Keil K. 2000. Microstucture of condensate Fe-Ni metal particles in the CH chondrite PAT 91546 (abstract #1445). 31st Lunar and Planetary Science Conference. CD-ROM.

Righter K., Campbell A. J., and Humayun M. 2005. Diffusion of trace elements in FeNi metal: Application to zoned metal grains in chondrites. *Geochimica et Cosmochimica Acta* 69:3145–3158.

Romig A. D., Jr., and Goldstein J. I. 1980. Determination of the Fe-Ni and Fe-Ni-P phase diagrams at low temperatures (700 to 300 °C). *Metallurgical Transactions* 11A:1151–1159.

Scott E. R. D. 1988. A new kind of primitive chondrite, Allan Hills 85085. *Earth and Planetary Science Letters* 91:1–18.

Smith B. A. and Goldstein J. I. 1977. The metallic microstructures and thermal histories of severely reheated chondrites. *Geochimica et Cosmochimica Acta* 41:1061–1072.

Vander Voort G. F., editor. 1992. *Metallography and microstructures.* ASM Handbook, vol. 9. Materials Park, Ohio: ASM International. 837 p.

Wasson J. T. and Kallemeyn G. W. 1990. Allan Hills 85085—A subchondritic meteorite of mixed nebula and regolithic heritage. *Earth and Planetary Science Letters* 101:148–161.

Weisberg M. K., Prinz M., and Nehru C. E. 1988. Petrology of ALH 85085: A chondrite with unique characteristics. *Earth and Planetary Science Letters* 91:19–32.

Weisberg M. K. and Prinz M. 1999. Zoned metal in the CR clan chondrites (abstract). 25th Symposium on Antarctic Meteorites. pp. 187–189.

Weisberg M. K., Prinz M., Clayton R. N., Mayeda T. K., Grady M. M., and Pillinger C. T. 1995. The CR chondrite clan. *Proceedings of the NIPR Symposium on Antarctic Meteorites* 8: 11–32.

Weisberg M. K., Prinz M., Clayton R. N., Mayeda T. K., Sugiura N., Zashu S., and Ebihara M. 2001. A new metal-rich chondrite grouplet. *Meteoritics & Planetary Science* 36:401–418.

Widge S. and Goldstein J. I. 1977. Redetermination of the Fe-rich portion of the Fe-Ni-Co phase diagram. *Metallurgical Transactions* 8A:309–315.

Yang J. and Goldstein J. I. 2005. The formation of the Widmanstätten structure in meteorites. *Meteoritics & Planetary Science* 40:239–253.

Yang J. and Goldstein J. I. 2006. Metallographic cooling rates of the IIIAB iron meteorites. *Geochimica et Cosmochimica Acta* 70: 3197–3215.